UNIVERSITY OF CALIFORNIA,
IRVINE

Computational modeling of the directionally-dependent leaflet properties of a bileaflet mitral bioprosthesis

THESIS

submitted in partial satisfaction of the requirements for the degree of

MASTER OF SCIENCE
In Biomedical Engineering

by

Joshua William Yu

Thesis Committee:
Professor Arash Kheradvar, Chair
Professor Elliot Botvinick
Associate Professor Anna Grosberg

2019

TABLE OF CONTENTS

LIST OF FIGURES

LIST OF TABLES

ABSTRACT OF THE THESIS

Computational modeling of the directionally-dependent leaflet properties of a bileaflet mitral bioprosthesis

By

Joshua William Yu

Master of Science in Biomedical Engineering

University of California, Irvine, 2019

Professor Arash Kheradvar, Chair

The bileaflet mitral valve is a highly complex organ in the body that regulates the blood that flows through the left atrium and into the left ventricle. It is designed to withstand decades of powerful forces within the pulsating chambers of the heart. The mitral valve's bileaflet structure distinctly possesses two leaflets rather than three, unlike the other cardiac valves. When compared to the trileaflet valves, bileaflet mitral bioprosthetics face significant challenges due to structural complexity—nonplanarity in annulus shape, asymmetrical geometry, and heavily oriented collagen fibers. Understanding the mechanical properties that affect mitral valve biomechanics is crucial for developing bileaflet bioprosthetic designs. By use of finite element (FE) modeling and Abaqus computational packages, this project investigates the geometrical and structural properties of bileaflet mitral bioprosthetics that contribute to a reduction in stresses along the edges of the leaflet. The resulting data illuminates how the saddle-shape of the mitral annulus and fiber orientation affects stress distributions of the leaflet during simulated pressures. Incorporation of a fiber-aligned constitutive model

contributes to significant variations in circumferential and radial stress/strains across the saddle-shaped bioprosthetic. Results indicate that circumferential stress is uniquely distributed away from the leaflet edges as an effect of the saddle-shape geometry. Future work using the knowledge gained from this project may use the correlation between the directionally-dependent tissue fibers and those stress/strain distributions to improve future mitral bileaflet bioprosthetic engineering designs.

INTRODUCTION

Understanding Biomechanics of Mitral Valves

Heart valves are crucial components of the cardiac cycle that ensure a unidirectional flow of blood throughout the heart. The main purpose of the mitral valve is to permit blood to flow from the left atrium to the left ventricle while preventing backflow when it is closed, according to [1]. The mitral valve is a unique case due to its bileaflet design. Whereas the aortic, pulmonary, and tricuspid valves feature trileaflet designs, the mitral valve has only two leaflets (or cusps), as described by [2]. There is no clear consensus on why the mitral valve developed into a bicuspid design instead of a tricuspid design like the other valves, according to [3]. Also, the bileaflet mitral valve, featuring a nonplanar saddle-shaped annulus and non-symmetrical geometry, is more structurally complex than the aortic or pulmonary valve [2]. As a result, most of the research on valve bioprosthetics has been directed towards trileaflet designs like the aortic and pulmonary valves, according to [1].

The trileaflet aortic valve is situated at the endpoint of the aorta, the largest blood vessel in the body, while the bileaflet mitral valve is situated between heart chambers. Thus, mitral replacements require more invasive techniques, like transapical insertion, when compared to aortic valves due to being positioned inside the heart and farther away from the primary blood vessels, according to [4]. In addition, the mitral annulus—the fibrous ring that connects to the mitral leaflets—is less circular, less rigid, and consequently more variable than the aortic annulus, making proper stent expansion of mitral bioprosthetics more difficult, as described in [5]. The mitral annulus is shaped like a three-dimensional saddle, meaning the surface of the structure curves hyperbolically

up in one direction, but also curves downward in the other, perpendicular direction (see Figure 1). Previous studies conducted by Padala, Kheradvar, Vergnat, and others have shown that the natural saddle shape of the mitral annulus contributes to reduced mitral annular strain [6], reduction in leaflet stress [3], and increased leaflet coaptation [7].

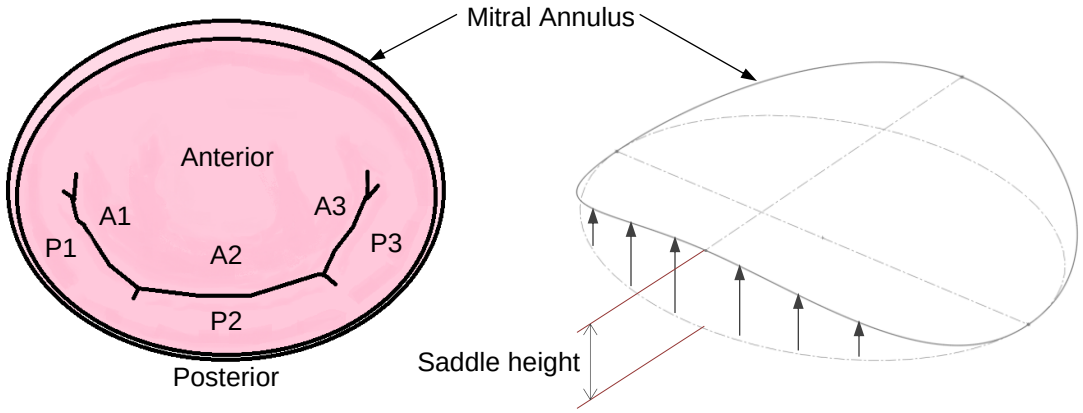

Figure 1: Three-Dimensional Shape of the Mitral Annulus Geometry

Adapted from Carpentier's Reconstructive Heart Surgery [8] and Prot's Finite element analysis of the mitral apparatus [9]. The bicuspid anatomy of the mitral valve is divided into regions: the anterior leaflet and the posterior leaflet [8]. Both of those are subdivided further into numbered regions: A1, A2, A3, P1, P2 and P3. AC and PC refer to the anterolateral and posteromedial commissures, respectively. The fibrous ring that surrounds the mitral valve, the mitral annulus, features nonplanarity in its geometry in a 3D saddle shape [9]. The saddle height reaches its apex at the P2 region of the leaflet.

Determining the effects of the saddle-shape on the stress experienced during valvular motion could shed light on the directionally-dependent properties of the valve leaflet tissue. Mitral valves feature distinct directionally-dependent mechanical properties as a result of the leaflet fiber configuration. Mitral valve leaflets are composed of collagen fibers that are oriented in the radial and circumferential direction, leading to anisotropic mechanical properties of the leaflets, as detailed in [1] and [10]. Understanding the biomechanics behind the bileaflet nature of the mitral valve, the saddle-shape of the annulus, and the fiber alignment of the leaflet tissue is crucial for the development of long-lasting bioprosthetic engineering designs.

Current Mitral Valve Research

Previous studies by Dr. Kheradvar and Falahatpisheh [3] have shown that leaflet stresses are focused around the annulus edges of the leaflet, reducing the durability of surgical implants and resulting in valvular failure over time. Across the biomedical field, various tests have been conducted on mitral structures examining the effects of fiber direction when it comes to mechanical stresses and strains. The orientation of these fibers in different layers throughout the depth of the valve leaflet has been shown to vary with respect to different loads, according to Alavi [10], [11]. Mitral valves under biaxial tests are known to exhibit large deformations and behave anisotropically, or directionally-dependent, as shown by May-Newman [12]. In other words, the stiffness of the valve differs depending on whether you measure it in the circumferential, radial, and axial directions. In-vitro research by M. Padala [6] has shown that the saddle curvature of the mitral annulus significantly reduces mechanical strains in the radial and circumferential directions during systolic valve closure. The influence of the valve structure's nonplanarity still is not well understood, especially during valvular motion. Tests such as Padala's [6] were conducted in vitro, and biaxial tests such as Billiar's [13] and May-Newman's [14] were done with sections of valve tissue in a fixed state.

Thus, there is a need for in-depth modeling of mitral bioprostheses to observe the effects of its saddle-shape geometry and anisotropicity during motion without the effects of tethering. Computational models can investigate the effects of both saddle curvature and fiber direction under simulated pressures that are unavailable in vitro. Investigating the leaflet mechanical properties of fiber direction is crucial for interpreting

the valve physiological function, inspecting potential modes of failure, and designing future bioprosthetic heart valves.

Current State-of-the-Art in Heart Valve Engineering

Constitutive modeling is crucial to the field of heart valve engineering. Analysis of the finite element models has led to breakthroughs in heart valve surgery, design of bioprosthetic valve replacements, and improving knowledge of how both normal and abnormal cardiac functions work, according to [15]. The field has exploded with research in the past few decades, and a variety of approaches have been put forth as theoretical best ways to model the complex nature of leaflet mechanics. Dr. Weinberg [15] describes the current state of heart valve engineering to fall into the following categories:

I. Rubber-derived models
II. Phenomological models
III. Transversely isotropic models
IV. Aligned fiber models
V. Unit-cell models

Of these, the transversely isotropic and aligned fiber models are most relevant to this paper. Common to all the listed models are the key assumptions that researchers take in order to develop constitutive models for the valves. Namely, heart valve tissue is modeled with the properties of a pseudoelastic, incompressible, anisotropic, and nonlinear material, according to [15]. Researchers have agreed, according to [16], that aligned fibers of the tissue result in anisotropic hyperelastic properties within physiological ranges of strain. In addition, [15] states that a majority portion of the tissue

volume is composed of water tightly bound to the solid matrix, leading to the assumption that the tissue is incompressible.

There are two major reasons why constitutive models are so difficult to develop for soft biological tissues of valve bioprosthetics. One is the miniature size of the valves. The second reason is the heterogenous fibrous structure of the valve leaflets, according to [13]. Biaxial testing performed by Billiar and Sacks [13] have shown that local fiber orientations are the dominant forces during leaflet deformation. Additionally, circumferential strains were recorded to be significantly smaller than radial strains, signifying a high amount of mechanical anisotropy in valve leaflets, as detailed in [13]. In other words, heart valve leaflets are measured to be stiffer in the circumferential direction when compared to the radial direction. Dr. Weinberg [15] further classifies approaches to tissue modeling into two main categories: structurally based models and invariant based models. The structurally based model described by Billiar and Sacks [17] allows incorporation of fiber directions by integration, and it has been shown to be accurate in aortic valve tissue. The invariant based model described by May-Newman and Yin [14] brings in the assumption of material transverse isotropy and has been shown to be applicable to mitral valve tissue. The invariant based model is less computationally intensive due to requiring less calculations when compared to the structurally based model, according to [16]. The transversely isotropic model verified by May-Newman and Yin [14] shows that the stress and deformation responses can be represented as a function of the first invariant and the stretch in the fiber direction, describing a strain energy function for mitral valve tissue.

Other studies have noted that very few researchers have incorporated the mechanical properties associated with layers and its effect on nonuniformity of stress distributions. Stella and Sacks [18] show that the distinct layers of the heart valve leaflets exhibit very different nonlinear and highly anisotropic mechanical behaviors. Whereas the leaflet tissue mechanical behavior was dominated by the fibrosa layer, the total radial tension was dominated by the ventricularis and experienced four times the stress of the fibrosa, as shown by [18]. In addition, the ventricularis was found to experience very high amounts of anisotropic behavior at low levels of stress and is dominated by circumferentially oriented collagen fibers at all strain levels. As a result, the initial loading phase of the ventricularis layer was deemed to be unable to be modeled as an isotropic material.

Dr. Wei Sun, Sacks, and Abad [19] have noted that previous finite element studies of prosthetic valves do not incorporate actual mechanical properties of bioprosthetic heart valves such as the geometry, the fibrous structural information, and interleaflet variability. Finite element models have been key in researching the effects of stress concentrations within the leaflet that accelerate the rate of tissue structural damage leading to calcification. However, there are many challenges associated with these numerical simulations because experimental measurements are difficult to validate at measurements close to actual bioprosthetic leaflet properties. When deciding element types in finite element studies, Dr. Wei Sun [19] notes that 3D brick elements encountered severe issues when modeling thin structures due to requiring 3D constitutive modeling, out-of-plane tissue properties not obtainable by experimental data, and difficulty in enforcing the condition of incompressibility. As bending damage is

a known cause of valvular mechanical failure, membrane elements are not used in Sun's study [19] due to being tension-only structures without bending effects. Shell elements are chosen as the finite element type of choice due to ease of enforcing the incompressibility constraint, inclusion of bending properties, and simplification of experimental tissue properties required for the constitutive model.

The biggest challenge for heart valve researchers in developing constitutive models is that heart valve tissue is thin, and thus it only can be thoroughly tested under planar tension. However, in native conditions, heart valve leaflets experience huge amounts of out-of-plane (nonplanar) and compressive stress, according to [15]. Therefore, it falls on engineers to design models using two-dimensional data to deal with complex three-dimensional behavior, which is not a simple task. Every model has its own flaw. Phenomological models have low amounts of verification with experimental data. Transversely isotropic models like Fung's only work with in-plane stress terms and cannot fully work in three dimensions. Lastly, other than the Stella and Sacks [18] constitutive model, none of them incorporate the mechanical distinctness of layers, according to [15]. All constitutive models for the purpose of finite element analysis have room for improvement, and it is ever more important for characterizing the deformation of leaflet tissue as a tool for designing better bioprosthetic valves.

METHODS

This study presents an investigation of how the bileaflet design, the saddle-shape of the mitral annulus, and the directionality of leaflet fibers affects stress distributions during opening and closing of the mitral valve. This project will test the effectiveness of

introducing a preferred orientation of collagen fibers in the mitral leaflets. To do so, mathematical models of strain energy potential that incorporate a dependence on fiber direction will be implemented into computational software. The amount of stress experienced in each direction will determine the effectiveness of incorporating optimized fiber alignment in bioprosthetic designs. It is expected that emulating the native fiber orientations of mitral valves in the form of anisotropic material properties will strengthen the mitral bioprosthesis, bringing it closer in nature to the natural leaflet.

The aims of this study are as follows: using numerical methods, simulate dynamic pressures on a saddle-shaped, bileaflet mitral bioprosthetic featuring anisotropicity and aligned fiber direction, examine opening and closing phases of motion for stress distributions, and draw conclusions from the study of stress/strain distributions resulting from the shape and constitutive models used. The goals of this study can be divided into three main parts:

I. Develop a finite element (FE) model for a bileaflet mitral valve bioprosthesis containing a 3D saddle-shaped annulus.
II. Introduce directionality of fibers to the leaflet portions of the mitral bioprosthesis in the form of anisotropic material properties using finite element analysis in ABAQUS software.
III. Compute biomechanical responses under pressure simulations and determine if the saddle geometry and fiber direction have a significant effect on the stress and strain distributions in the leaflets.

Part I: The Case for a FE Modeled, Saddle-Shaped Bioprosthetic

The FE design of the bioprosthetic will be modeled after the saddle-shape that has been well-characterized of the native mitral valve. The reason for including the saddle-shaped annulus is detailed in previous studies by Kheradvar and Falahatpisheh [3]. It was shown that shape of the dynamic annulus contributed greatly to reduction of stress along the tips of the leaflets when compared to a flat, rigid annulus. In addition, M. Padala's studies [6] have shown that systolic strains have been reduced in the P2 segment of the mitral leaflet as a result of the saddle-shaped mitral annulus in both the radial and circumferential directions. Minimization of stress and strain along the leaflet tips verifies the usage of a saddle-shaped annulus in bioprosthetic designs.

Mitral Valve Assumptions

In FE modeling of the geometrically unique shape of the mitral bioprosthesis, complexity is dealt with via the engineering methodology of best-fit approximations. As described in [5], the anatomy of the mitral valve can be simplified as a two-part bileaflet structure, featuring a saddle-shaped annulus and a roughly circular base. As an approximation of the bicuspid valve, it will feature symmetric properties across the coronal and sagittal planes; thus, the leaflet portions will be divided into the anterior and posterior regions, and further sub-divided into quarters. The anterior and posterior leaflets of the mitral valve should not be strictly named as such, due to the mitral valve's oblique position in the heart, according to [5]. Nevertheless, for the proposed bioprosthetic, the vague symmetry of the two native leaflets will be considered to have absolute symmetry, equating the properties of the anterior and posterior leaflets. These

approximations will serve the purpose of bringing the focus solely towards the overall influence of shape and fiber alignment on how the FE model responds to high amounts of pressure.

According to the current state-of-the-art research conducted by similar studies, the following properties will be assumed for all following simulations. The leaflet material will enforce hyperelasticity, incompressibility, and transverse isotropicity when modelled in ABAQUS, as used by [20]. Uniform thickness will be assumed across the entire leaflet surface shell. While it is known, according to [21], that the mitral leaflets are heterogeneous in material properties across different regions of the structure, for this study, leaflet homogeneity will be assumed as a simplification of the native mitral valve to help quantify data during analysis.

FE Modeling

Like many biological tissues, stress and strain measurements are unable to be practically measured using the native geometry of valve leaflets in the natural state of loading and boundary conditions, as explained in [12]. Therefore, predictive methods of obtaining stress distributions by use of constitutive modeling are a way to obtain measurements to help validate future experimental data. For complex 3D geometries such as mitral valve leaflets, FE models are an ideal numerical method for determining stress and strain data.

The saddle geometry of the valve results in a leaflet surface edge that curves up in one direction but curves downwards in the other. This divergent curvature originates at a critical point called the saddle point, and it is akin to the inflection point of a hyperbolic

curve, but in 3D space. The FE model presented in this study is based on previous models created by Kheradvar and Falahatpisheh [3] and features several saddle points at the base of the leaflets, forming a complex saddle surface for each side of the bicuspid valve.

For the process of developing a robust FE model, the tools provided by Solidworks were chosen as the method of construction, with the intent to import said geometry over to Abaqus for stress analysis. The curved surface of the leaflet was handled by lofting two sketch profiles across 3D space and guided by curves to create the unique saddle geometry of the bileaflet bioprosthetic design (see Figure 2). The leaflets were first designed in quarters and then mirrored across the planes of symmetry to create the full geometry of the valve. A similar method was used for the frame of the leaflet model. The outer edge's curve served as the sweep path of a circular profile, creating a frame that is fully in contact to the annulus edge throughout the entire model. The following figures (Figure 2, 3, and 4) lay out the specifications for the bileaflet bioprosthetic design.

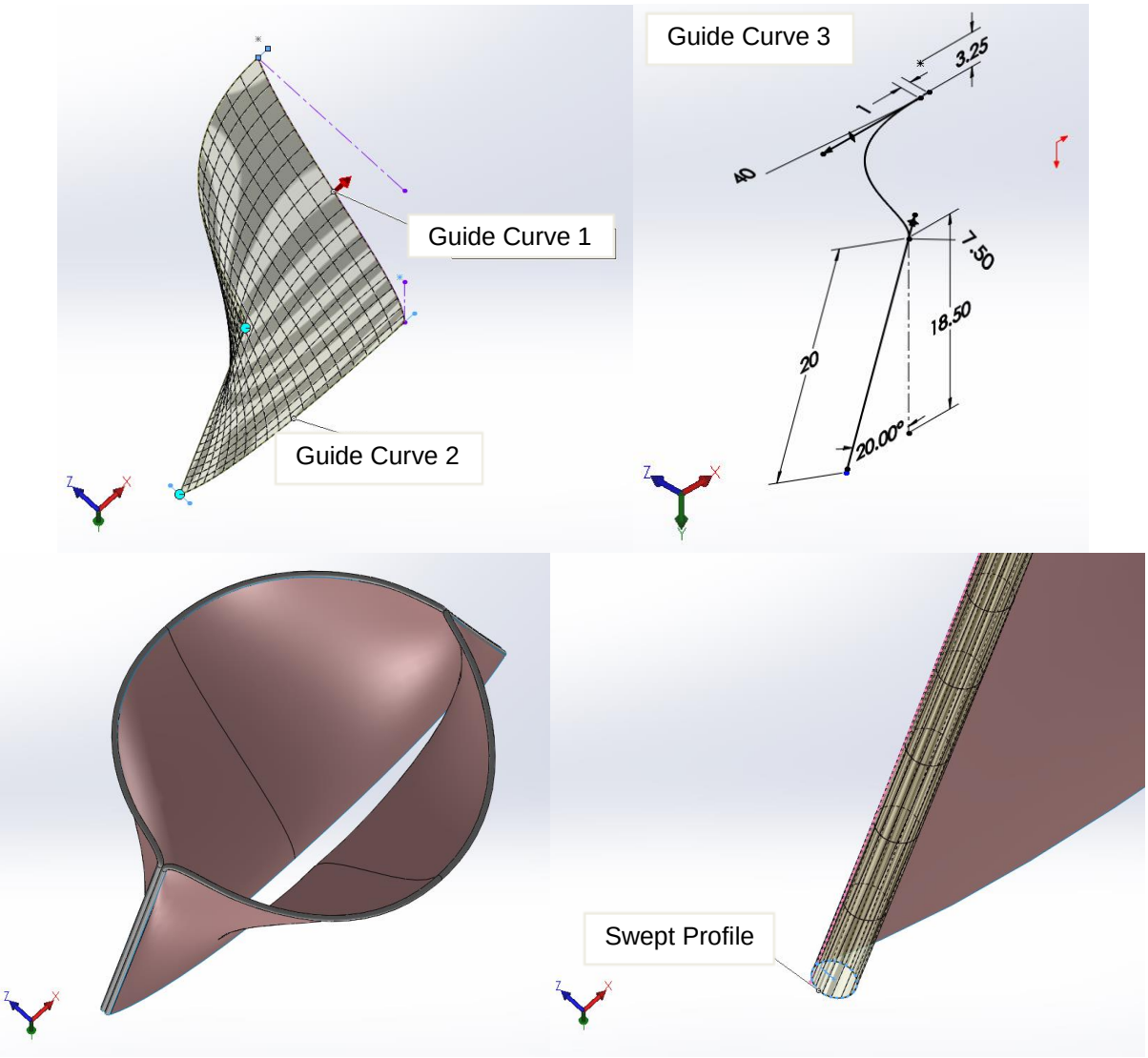

Figure 2: Solidworks FE Modeling

Construction of 3D geometry was handled by sketching guide curves and paths as guided splines for the surface loft and surface sweep feature tools. The loft tool creates the surface between two 3D sketches, while the sweep tool constructs a circular profile along a path, following it from start to end. All views here are from roughly the same perspective, looking down at the bileaflet structure from the Left Atrium and entering the Left Ventricle.

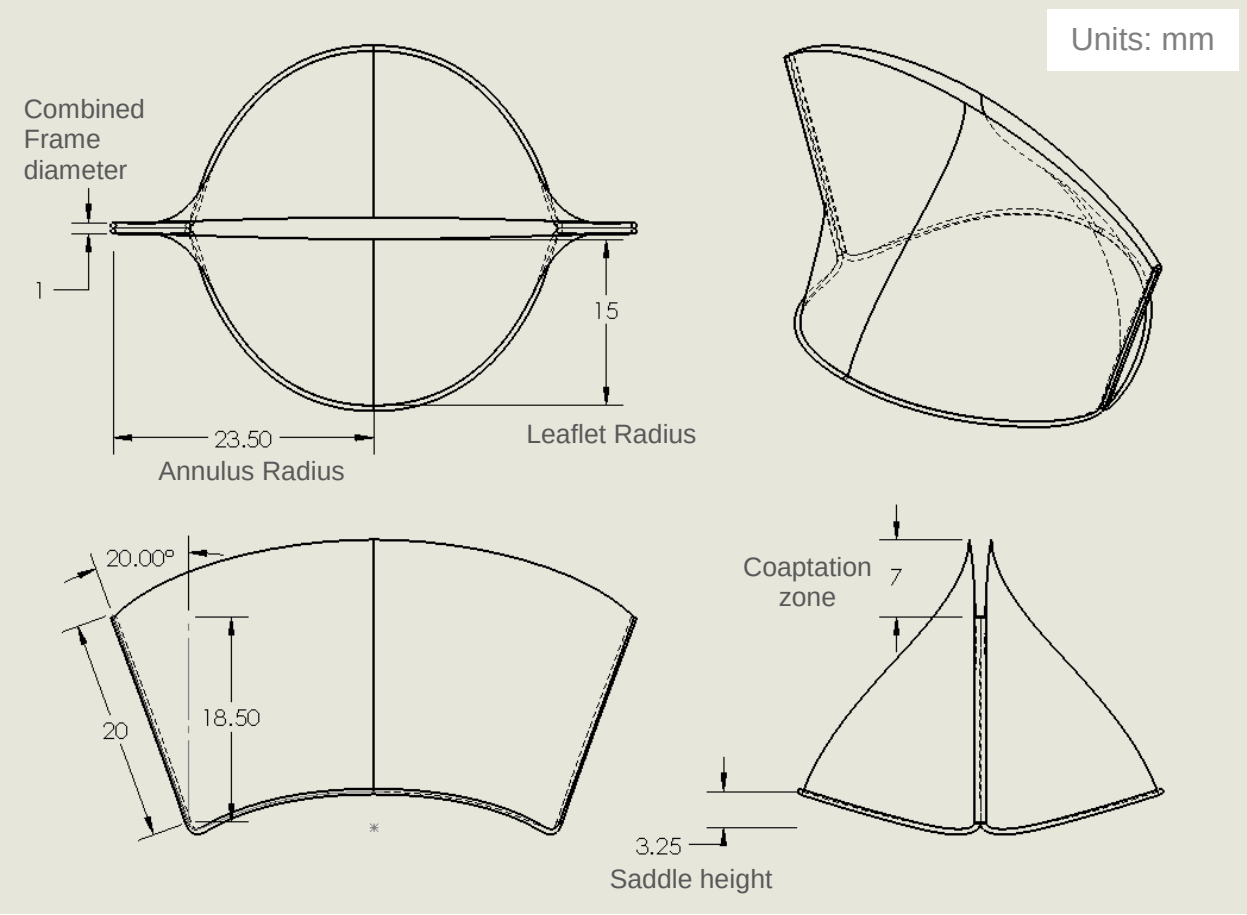

Figure 3: Model dimensions of the bioprosthesis design.

Solidworks drawing of the mitral bileaflet bioprosthesis design, displaying dimensions in millimeters. Note that the valve is pictured here upside-down—in the body, it would be viewed with the narrower opening facing towards the left ventricle, with blood flowing in from the left atrium through the larger circular opening. The coaptation zone is labeled at the region where the two leaflet halves are in contact during leaflet closure. Views are displayed in the order, from left to right: Top, Isometric, Front, and Side.

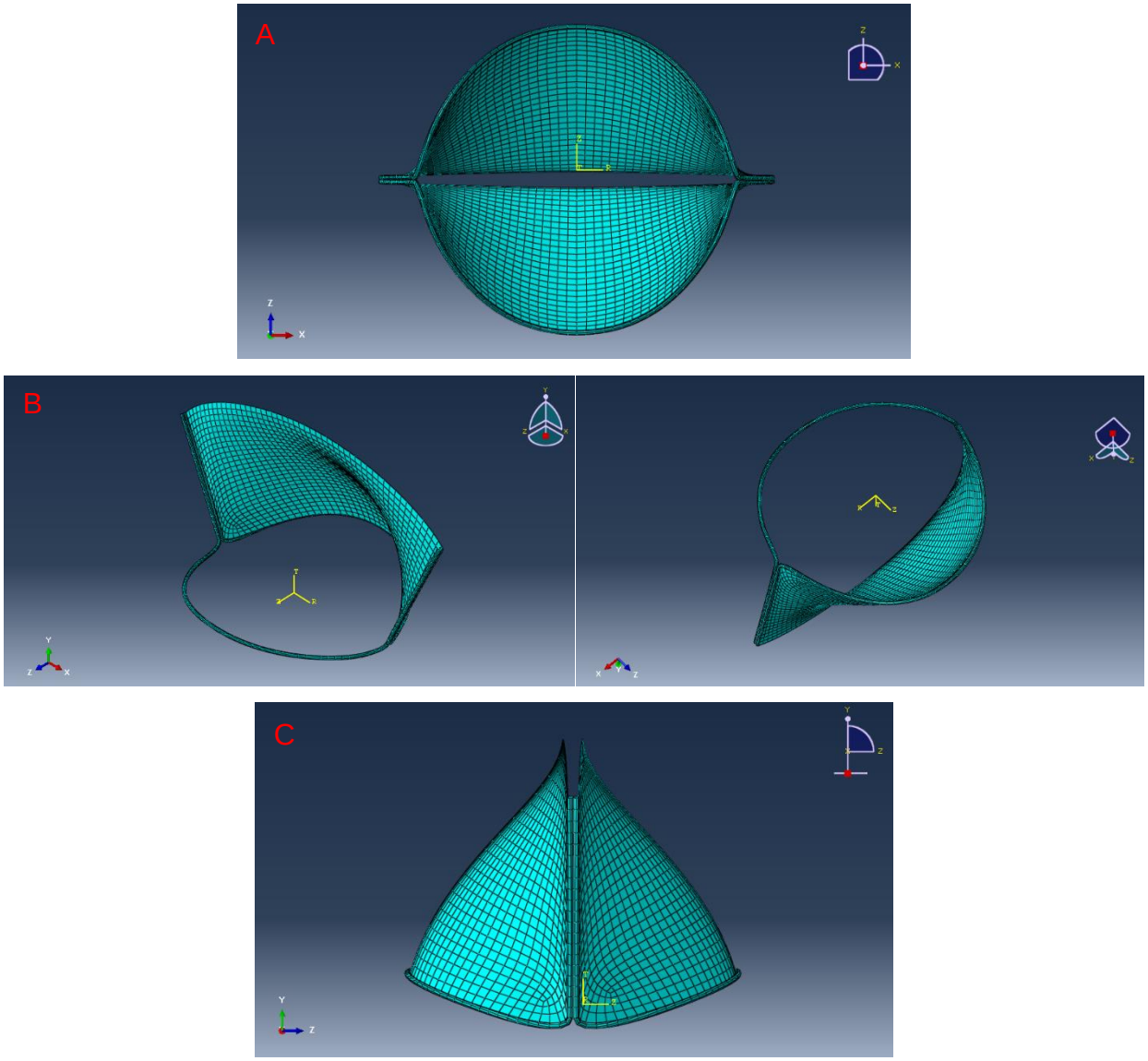

Figure 4: Mesh Elements: Quad-Structured (Leaflet), Quad-Sweep (Frame)

A. Overhead view, perspective of Left Atrium. Meshed using ABAQUS/Explicit element library. Leaflet mesh thickness is not rendered in this image or the following images.
B. Two Isometric views. Four combined leaflet quarters tied to a nitinol frame with constraints held at the edges. One leaflet half hidden from view.
C. Side View, parallel to sagittal plane. Mesh Element Controls: Four-node shell element (S4R), featuring linear geometric order, reduced integration, hourglass control, and finite membrane strain on a four-sided shell element.

On Nitinol and the Shape Memory Effect

The valve will be supported by a nitinol frame that can bend and deform along with the saddle-shape of the bioprosthetic (see Figure 5). The inclusion of a flexible, biocompatible, and shape-memory material as a support allows for non-invasive surgical implants to the body without compromising the strength or biocompatibility of the bioprosthetic. The shape of the nitinol frame will closely follow the saddle-shape curvature of the mitral annulus, assisting in the valve's structural integrity while opening and closing once the bioprosthetic is deployed within the body. The side prongs assist with keeping the bileaflet structure from collapsing in on itself, akin to the role of the chordae tendineae, as explained by [3].

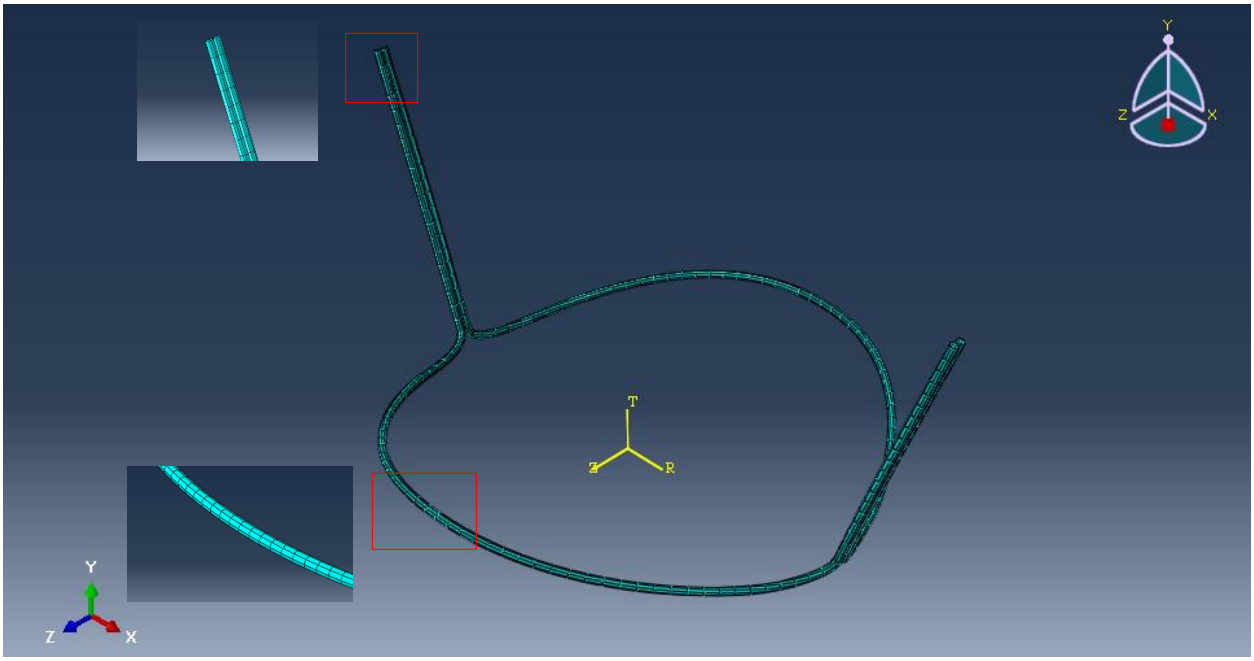

Figure 5: Mesh of the Nitinol-Based Saddle Geometry

Mesh Element: Quad-Sweep (Type S4R) shown in close-up views of the displayed areas. The meshing was performed in Abaqus. The nitinol wire follows the mitral annulus saddle geometry. As the nitinol frame moves, the enclosed leaflet must also deform and interact with it. Mitigation of the stress caused by said deformation is theorized to rely heavily on the saddle-shape geometry.

User material (UMAT) subroutines were used to model the frame material with the shape memory alloy, Nitinol. Nitinol is an alloy of the elements Nickel and Titanium, and it possesses the ability to reconstruct its shape under certain temperatures [22]. The phase transformation between its low temperature form (martensite, 291 to 271 K) and high temperature form (austenite, 295 to 315 K) provide Nitinol with its shape-memory and superelastic properties (see Table 1). Martensite is weaker and can be easily deformed; however, when heated above its transformation temperature to austenite, it recovers its original shape with great force [22]. As internal body temperature is approximately 310 K, nitinol begins its phase transformation to austenite within the body, remembering its pre-deformed shape. The exact temperature at which the material transforms can be specified by alloy composition and heat treatment techniques [22]. Nitinol is strong, ductile, biocompatible, and very resistant to corrosion, making it an ideal material for leaflet support. In addition, because nitinol features superelastic properties at temperatures slightly above its transformation temperature, it is well suited for designing flexible delivery methods into the body.

UMAT Subroutine Implementation

The UMAT subroutine is provided with inputs such as stress, solution dependent variables (SDVs), temperature, and strain. After calculating the input and its effect on the material, it outputs updated values of the stress tensors, SDVs, and stiffness tensors (stiffness matrix). Lagoudas [23] describes the step where UMAT subroutine is executed in the Abaqus flowchart (see Figure 6). The UMAT is incorporated into the calculation of stress σ and the partial derivative of the change in stress over strain. In

this way, each iteration of the program calls back the material parameter values and updates them as necessary in every step of the analysis. This implementation of UMAT is included in this study to accommodate the dynamic elastic modulus of Nitinol.

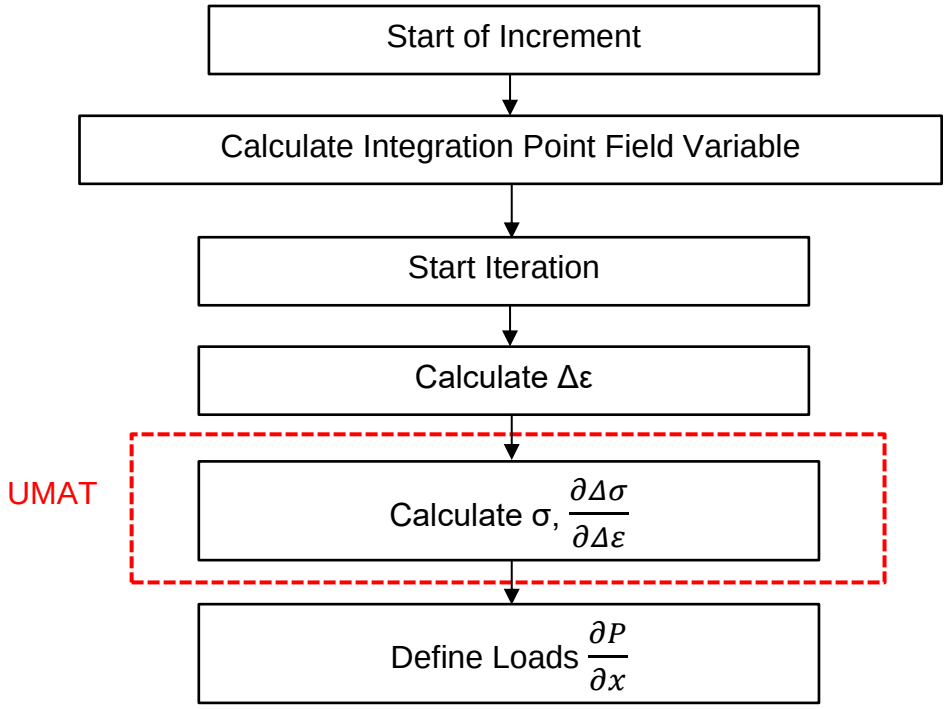

Figure 6: UMAT Subroutine Integration Flowchart

Flowchart detailing the steps Abaqus takes during analysis. Adapted from Ahmad's Writing User Subroutines in Abaqus [39]. The UMAT subroutine is implemented at the step in software analysis during calculations of the stress and the elastic modulus.

UMAT subroutines were coded in Fortran, and the code includes a thermomechanical constitutive model. The implementation of the UMAT subroutine into the Abaqus program is detailed in Lagoudas' Shape-Memory Alloy Manual [23]. A more detailed description of table values can be found in Appendix A. For a more detailed description of the model, see Appendix B. A table of parameters relevant to the study are listed below, in Table 1.

Values for the Young's modulus (elastic stiffness) of the Nitinol alloys were obtained by performing uniaxial pseudoelastic tests as detailed by Lagoudas [23] and Qidwai [24], where the stiffness of the austenite and martensite forms are obtained by measuring the slope of the stress-strain curve and the beginning of loading for austenite and beginning of unloading for martensite. Also, in studies conducted by Lagoudas [23] and Qidwai [24], the thermal expansion coefficient was obtained by standard tests at low and high temperatures for both phases of the material. Transformation temperatures were obtained with a Differential Scanning Colorimeter test (DSC). The maximum transformation strain required a pseudoelastic test, while the stress influence coefficients are observed by the stress-temperature phase diagram and pseudoelastic test [23].

Table 1: Nitinol Shape Memory Alloy Material Parameters—Austenite & Martensite

NiTi Material Parameter Description	Value
E^A , E^M : Young's modulus ("A"-austenite, "M"-martensite)	70,000 MPa, 30,000 MPa
v : Poisson's ratio (equal for both)	0.33
α^A , α^M : thermal expansion coefficient	22E-6 K^{-1}, 10E-6 K^{-1}
A^{0f} , A^{0s} , M^{0s} , M^{0f} : start and finish temperatures at zero stress	315 K, 295 K, 291 K, 271 K
H : maximum transformation strain	0.05
$\rho\Delta s^A$, $\rho\Delta s^M$: stress influence coefficients	-0.35 MPa K^{-1}

*Adapted from Qidwai [24] and Lagoudas [23].

Next, material properties are assigned to each separate section of the model accordingly: leaflet tissue, nitinol, etc. Also, a local orientation system must also be specified, in the case of fiber aligned material properties. The orientation axis was placed at the bottom center of the model assembly by means of cylindrical coordinates in the Abaqus property module.

Part II: The Case for a Transversely Isotropic, Fiber Aligned Bioprosthetic Model

Bioprosthetics are an imitation of tissue, and thus they must be modeled accordingly. Like many complex materials, tissue is an anisotropic material, meaning many of its properties are measured at different quantities depending on the direction said measurements are taken. The anisotropic properties of the valve material can be represented by May-Newman's [12] transversely isotropic model of hyperelastic constitutive laws, which is an adaptation based on the Fung-Anisotropic Hyperelastic model. May-Newman's [12] constitutive model was derived from observing the alignment of collagen fiber layers that are highly oriented within the valve microstructure. In more recent years, the isotropic Holzapfel-Gasser-Ogden model [25] has seen prevalent use in FE studies of bioprosthetic leaflet mechanics by applying a numerical degree of local fiber orientation, as detailed by Pham [26]. One way of applying fiber direction directly to the bioprosthetic model is adjusting material properties by providing matrix sets of directional data in finite element programs. The programs can then apply the data to the model in 3D space to emulate the existence of fiber alignment during the computational analysis.

Anisotropic Hyperelastic Constitutive Model

Applying strain energy functions to soft biological tissues, including the mitral valve, was advocated early on by Y.C. Fung for use in bioprosthetic studies, according to May-Newman [12]. Consequently, a variety of models were developed that approximated the leaflet tissue as an anisotropic, hyperelastic material, including the more modern Holzapfel-Gasser-Ogden model [25]. The following constitutive model will

take inspiration from the basis of the Fung-Anisotropic form, be simplified into a transversely isotropic form, and be fully implemented into Abaqus using the hyperelastic Holzapfel-Gasser-Ogden model.

For the leaflet portions of the FE model, material modeling is difficult, as soft tissues defy most known material models. Soft tissues exhibit complex mechanical behavior: anisotropic properties, a high degree of nonlinearity in stress-strain curves, large deformations, material coupling, and more, as detailed in [27]. For this study, the mitral leaflet material properties are assumed to exhibit extremely nonlinear and hyperelastic behavior under stress-strain conditions.

According to the literature, the Fung-Anisotropic Hyperelastic model, proposed by Y.C. Fung, is suitable for describing nonlinear behaviors of soft biological tissues under finite deformations. According to Ateshian [28], it is also very suitable for modeling materials that undergo large anisotropic and nonlinear elastic behavior; it allows for optional energy dissipation and stress softening effects for soft, rubber-like materials. Therefore, as a generalized form of modeling the elastic strain energy function, it is suitable for this study's implementation into the FE model.

Under large deformations, hyperelastic materials exhibit highly anisotropic and nonlinear elastic behavior due to microstructure rearrangements, such as reorientation of the fiber directions due to deformation. Anisotropic behavior follows the inclusion of directionally dependent properties when measured in multiple directions—for example, circumferential, radial, and axial orientations. Thus, simulation of these nonlinear strain effects on mitral valve tissue requires accompaniment by geometric nonlinearity in every step in analysis due to reliance on finite-strain applications.

Hyperelastic materials are described in terms of a “strain energy density function,” *W*, which is defined as the strain energy stored in the material per unit volume as a function of deformation at that point of the material. There are two different ways to represent the strain energy function of anisotropic hyperelastic materials: strain-based and invariant-based. In strain-based formulations, the strain energy function is expressed directly in components a strain tensor, ex. Green strain tensor $\boldsymbol{U} = (\varepsilon^G)$. However, in invariant-based formulations, the strain energy function is expressed directly in terms of the invariants of the deformation tensor and fiber directions, according to [12].

The direction of fibers is characterized by the unit vectors $\boldsymbol{N}$ in the circumferential, radial, and axial orientations while the material is undeformed. Thus, the “strain energy potential” *W* depends on deformation and fiber directions together:

$$W = W(\boldsymbol{I_1}, \alpha)$$

$$\text{where } \alpha^2 = \boldsymbol{N} \cdot \boldsymbol{C} \cdot \boldsymbol{N} \text{ and } \boldsymbol{I_1} = Tr(\boldsymbol{C})$$

where **C** is the fourth-order deformation tensor. $\boldsymbol{I_1}$ is the first invariant of **C**, as described by May-Newman [14].

In other words, it will assume that the strain energy depends not only on deformation, but also on the fiber directions. Due to this project’s focus on the effects of fiber alignment, the general Fung-Anisotropic form will be used, represented with an invariant-based strain energy function.

Strain energy function (Fung), in accordance with [14]:

$$W = c_0(\exp(Q) - 1)$$

$$Q = c_1(\boldsymbol{I_1} - 3)^2 + c_2(\alpha - 1)^4$$

$\boldsymbol{I}_1$ is the first invariant of the deformation tensor, **C**.

Hyperelasticity describes a constitutive model for an ideally elastic material, and its stress-strain relationship can be calculated using the strain energy density function. In this project, material properties specified by the Fung-Anisotropic Hyperelastic model will require large matrices full of orientation data, including fourth-order elasticity tensors. Tensors are geometric objects that describe linear relationships between vectors, scalars, and other tensors. They are often used as a framework to help solve nonlinear systems—for example, those involving stress, elasticity, or fluid mechanics. A fourth order tensor is a higher order tensor with 81 components.

Cauchy Stress Tensor, from [29]:

$$[\sigma] = [C][\varepsilon]$$

Where **C** is a fourth-order tensor called the Elasticity tensor (or Stiffness tensor). It is a linear map between the second order tensors **σ** and **ε**. Each component of the tensor represents the resistance of a material to deformation in different directions, namely the circumferential, radial, and axial orientations of the mitral leaflet. The fourth-order symmetric tensor (Figure 7) contains all components required for a fully anisotropic material.

$$\begin{bmatrix}\sigma_{11}\\ \sigma_{22}\\ \sigma_{33}\\ \sigma_{23}\\ \sigma_{13}\\ \sigma_{12}\end{bmatrix} = \begin{bmatrix} C_{1111} & C_{1122} & C_{1133} & C_{1123} & C_{1113} & C_{1112} \\ & C_{2222} & C_{2233} & C_{2223} & C_{2213} & C_{2212} \\ & & C_{3333} & C_{3323} & C_{3313} & C_{3312} \\ & & & C_{2323} & C_{2313} & C_{2312} \\ & symm & & & C_{1313} & C_{1312} \\ & & & & & C_{1212} \end{bmatrix} x \begin{bmatrix}\varepsilon_{11}\\ \varepsilon_{22}\\ \varepsilon_{33}\\ 2\varepsilon_{23}\\ 2\varepsilon_{13}\\ 2\varepsilon_{12}\end{bmatrix}$$

symm → $C_{ij\,kl} = C_{kl\,ij}$

Figure 7: Matrix form, Fourth-order Tensor
Fully anisotropic stress tensor. Components 1, 2, and 3 refer to axes for circumferential, radial, and axial orientations of the tensor. Adapted from Irgens [29].

In Abaqus documentation [30], adding a temperature component to the strain energy potential gives:

$$W = \frac{c}{2}(\exp(Q) - 1) + \frac{1}{D}$$

Where $Q = \varepsilon_{ij} \cdot C_{ijkl} \cdot \varepsilon_{kl}$

The stress tensor **σ** is defined as a force over an area, meaning the units are in terms of pressure (Pa, or N/m^2). It is analogous to the restoring force **F** in Hooke's Law, as detailed in [29]. The strain tensor **ε** contains dimensionless components. It is equivalent to the displacement **x** in Hooke's law, defined as the displacement over distance. Thus, all matrix elements of $\boldsymbol{C_{ijkl}}$ have the units of pressure.

Transversely Isotropic Hyperelastic Constitutive Model

In Abaqus, the matrix data inputs can be simplified to a Fung-Orthotropic model, which assumes isotropic behavior in the three directionally-dependent axes of the tensor. In other words, a transversely isotropic model can be used for soft tissues,

according to [31], as a simplification assuming leaflet homogeneity in those specified orientations. Thus, the coupling terms that describe the relation between irrelevant terms can be reduced to sparse data entries. The elasticity Tensor, Stiffness Tensor **C**, can be represented using two major parameters, as shown in Figure 8.

$$\begin{bmatrix}\sigma_{11}\\ \sigma_{22}\\ \sigma_{33}\\ \sigma_{23}\\ \sigma_{13}\\ \sigma_{12}\end{bmatrix} = \begin{bmatrix}\lambda_{11}+2\mu_1 & \lambda_{12} & \lambda_{13} & 0 & 0 & 0\\ \lambda_{12} & \lambda_{22}+2\mu_2 & \lambda_{23} & 0 & 0 & 0\\ \lambda_{13} & \lambda_{23} & \lambda_{33}+2\mu_3 & 0 & 0 & 0\\ 0 & 0 & 0 & {}^1/_2(\mu_2+\mu_3) & 0 & 0\\ 0 & 0 & 0 & 0 & {}^1/_2(\mu_3+\mu_1) & 0\\ 0 & 0 & 0 & 0 & 0 & {}^1/_2(\mu_1+\mu_2)\end{bmatrix} x \begin{bmatrix}\varepsilon_{11}\\ \varepsilon_{22}\\ \varepsilon_{33}\\ 2\varepsilon_{23}\\ 2\varepsilon_{13}\\ 2\varepsilon_{12}\end{bmatrix}$$

Figure 8: Abaqus implementation of Fung-Anisotropic material properties.
Adapted from Ateshian [28]. The fourth order deformation tensor takes the dependency of the strain energy function on the fiber direction into account. This is a simplification of the fully anisotropic stiffness tensor into an orthotropic tensor, reducing the number of variables needed from 21 to 9.

- $\boldsymbol{\lambda_{ab}}$– Lamé first parameter
- $\boldsymbol{\mu_a}$ – shear moduli (Lamé second parameter)

There are nine constants - $\lambda_{11}, \lambda_{22}, \lambda_{33}, \lambda_{23}, \lambda_{13}, \lambda_{12}, \mu_1, \mu_2, \mu_3$.These nine material constants make up the constitutive relation, as described by Ateshian [28]. The following equations describe the two Lamé parameters in terms of the Young's Modulus (E) and the Poisson's ratio (v), as given by [32].

$$\lambda = \frac{Ev}{(1+v)(1-2v)}$$

$$\mu = \frac{E}{2(1+v)}$$

Young's Modulus E_i varies depending on Orientation (i = 1, 2, 3). Orientation refers to the circumferential, radial, and axial directions. The mitral valve will assume a uniform Poisson's ratio across all the leaflet surface. The mitral annulus has evidence pointing towards a greater stiffness in the circumferential direction (parallel to the annulus

edges) than the radial direction, according to [19]. To apply that to the Fung-Anisotropic model in Abaqus, a cylindrical coordinate system is specified for the material orientation properties of the assembly.

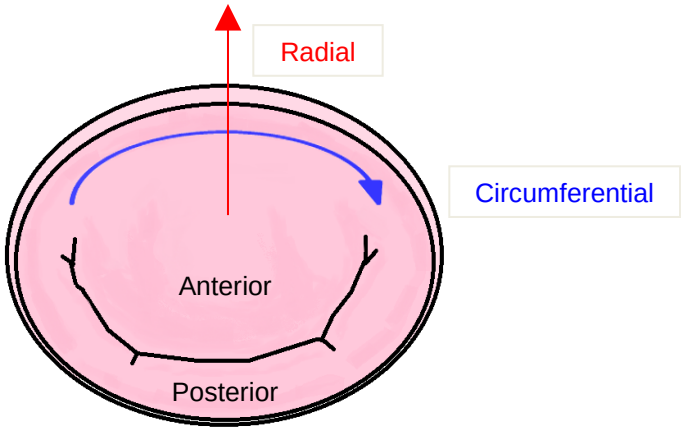

Figure 9: Diagram of circumferential and radial directions on a leaflet model

Adapted from Carpentier's Reconstructive Valve Surgery [8]. Transversely isotropic stresses assume rotational symmetry of the stress distribution, meaning that rotating the model around the central radial axis will not change the solid mechanics of the model. The radial direction extends perpendicular to the leaflet surface. The circumferential direction is parallel to the base of the mitral annulus. The axial direction is parallel to the leaflet edge and is not pictured in this image. It is possible to simplify the mitral model in this way due to the annulus shape and general approximations of blood flow through the valve geometry [8].

Thus, the number of parameters can be simplified further by removing the dependency on the axial directions and focusing on two orientations: the radial and circumferential directions. The amount required for the constitutive model has been reduced to five.

Table 2: Anisotropic Mitral Valve parameters for the Anterior and Posterior Leaflet

Variable	Description	Value	Units
$E_{1(\mathrm{AL})}$	Young's Modulus	6.2	MPa
$E_{2(\mathrm{AL})}$	Young's Modulus	2.1	MPa
$E_{1(\mathrm{PL})}$	Young's Modulus	2.35	MPa
$E_{2(\mathrm{PL})}$	Young's Modulus	1.89	MPa
v	Poisson's Ratio	0.49	Dimensionless

*Values adapted from studies conducted by Pouch [33]. 1- Circumferential, 2- Radial Young's Modulus and Poisson's ratio values to be used for the mitral bioprosthesis.

Fiber-Aligned Holzapfel-Gasser-Ogden Constitutive Model

The Holzapfel-Gasser-Ogden model describes an invariant based strain energy potential used to model fiber distributions in arterial tissues. It was proposed by Holzapfel, Gasser, and Ogden [25] to describe an orthotropic constitutive law for a fiber reinforced material, and it is based on a cylindrical coordinate system. Though it was intended for describing arterial tissue, it is now used broadly across a variety of soft biological materials, like valve leaflet tissue. The strain energy potential is described by:

$$U = C_{10}\left(\bar{I}_1 - 3\right) + \frac{1}{D}\left(\frac{\left(J^{el}\right)^2 - 1}{2} - \ln J^{el}\right) + \frac{k_1}{2k_2}\sum_{\alpha=1}^{N}\left\{\exp\left[k_2\langle \bar{E}_\alpha\rangle^2\right] - 1\right\},$$

$$\bar{E}_\alpha \overset{\text{def}}{=} \kappa\left(\bar{I}_1 - 3\right) + (1 - 3\kappa)\left(\bar{I}_{4(\alpha\alpha)} - 1\right),$$

where U is the strain energy per unit of reference volume. The equation format was adapted from the online Abaqus 6.13 documentation [30]. C10 describes the matrix stiffness, D defines the incompressibility, and k1 and k2 are parameters that relate to fiber stiffness (See Table 3). The model assumes a dispersion of fibers about a preferred orientation within the tissue. Alignment of fibers is designated by the term κ $(0 \leq \kappa \leq 1/3)$. A value of 0 indicates perfect alignment of fibers in the preferred direction, while a value of 1/3 indicates that the material is perfectly isotropic [26]. Applying this constitutive model in Abaqus will characterize the fiber orientation of native mitral tissue. The anisotropic properties of the mitral valve tissue resulting from this constitutive model will help describe the fiber aligned biomechanics of the bileaflet bioprosthetic design.

Table 3: List of relevant Abaqus input terms

Component	Description	Value	Units
μ_1	Shear modulus (circumferential)	2.08	N/mm^2 [MPa]
μ_2	Shear modulus (radial)	0.705	N/mm^2 [MPa]
ν	Poisson's ratio	0.49	Dimensionless
λ_{11}	Lamé constant (circumferential)	102	N/mm^2 [MPa]
λ_{22}	Lamé constant (radial)	34.5	N/mm^2 [MPa]
c01	Material constant	33.191	N/mm^2 [MPa]
c10	Material constant	0.101	N/mm^2 [MPa]
D	Incompressibility parameter	7 x 10^{-4}	mm^2/N [MPa^{-1}]
$k1$	Fiber stiffness	10.756	N/mm^2 [MPa]
$k2$	Nonlinear stiffness	48.495	N/mm^2 [MPa]
κ	Dispersion of fibers	0.089	Dimensionless

*Values adapted from Pham [26] and Pouch [33]

- $c01, c10$ – material coefficient (Units of F*L^{-2}) [MPa] - describes the shear behavior of a material. The lower the number, the softer the material.
- **D** (Units of F^{-1}L^2) [MPa^{-1}] "inverse material bulk modulus K_0" – describes the resistance of a material to compressibility, defined as the ratio of the infinitesimal pressure increase to the resulting relative decrease of the volume. D is given by the relationship $K_0 = 2/D$. Inverse of the bulk modulus (1/Pa) gives the compressibility of a material. It is set to 0 if the material is incompressible. According to Masugata [34], the bulk modulus (K_0) of myocytes is measured to be approximately 2.87 GPa.

Part III: Computational Analysis of the FE model in ABAQUS

Combining both Part I and II develops the groundwork for Part III. The FE model, which includes the saddle-shaped mitral annulus and the nitinol frame, is constructed in an Abaqus assembly and pressure simulations are applied to the combined model. To establish the biomechanical properties of the leaflet, directionally-dependent constitutive models are applied as parameters of the mesh elements. Conducting the simulation tests requires an establishment of the force side of the mathematical equation—in this case, pressure from one side of the mitral valve to the other. On the receiving side is the

Left Ventricle, where the pressures are traditionally higher than that of the Left Atrium. However, during the diastole phase of the cardiac cycle, the pressure in the Left Ventricle drops and stays at a constant pressure below that of the Left Atrium (see Figure 10). This negative pressure in the perspective of the Left Ventricle forms the basis for the events that allow the mitral valve to open, thereby allowing blood to fill the Left Ventricle.

Forces used in simulations – Pressures in the Cardiac Chambers

Applying pressure to the model is done through a series of steps—for opening of the valve during diastole and closing of the valve during systole. The pressure boundary condition is applied as a ramp, nonlinear geometry is applied, and pressure distribution is assumed to be uniform across the leaflet surface, as shown in Figure 11. Pressure homogeneity is enforced as a simplification of the native behavior of the forces exerted on the mitral valve leaflet. Additionally, pressures applied to the leaflet will not be adjusted to account for any changes in leaflet thickness throughout the surface. The reasoning behind this decision is to heavily focus on the biomechanics of the leaflet fiber distribution and geometry, rather than leaflet thickness. Stresses experienced by the leaflet will be monitored at the states of maximal opening and full valve closure.

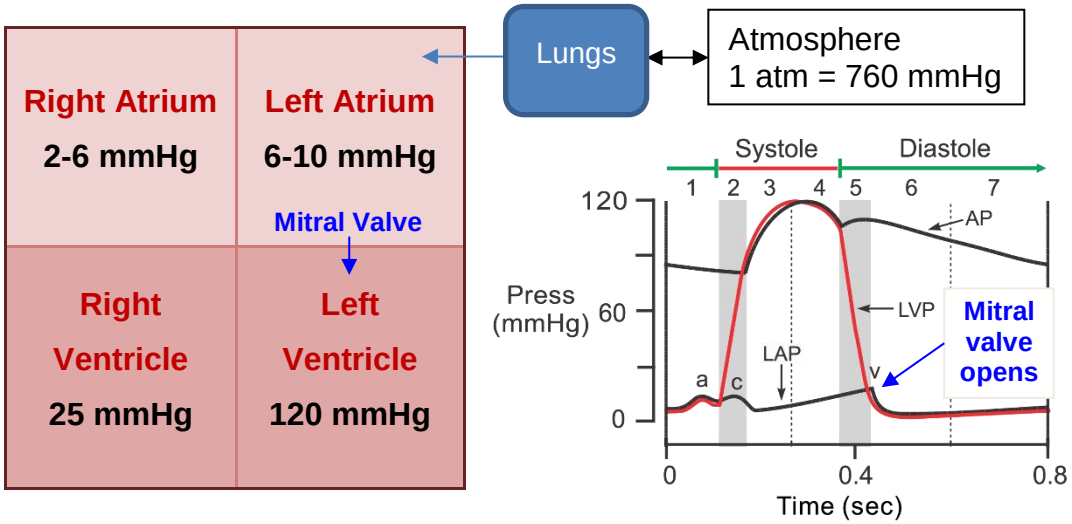

Figure 10: Negative Pressure Suction in the Cardiac Chambers

Adapted from Klabunde's Cardiovascular Physiology Concepts [35]. According to [36], peak transvalvular pressure: 120 mmHg. Pressure difference from the Left Atrium to the Left Ventricle can be approximated to 100 mmHg $(100\ mmHg\ =\ 0.0133\ MPa)$. As described in [35], the cardiac cycle chart displays the changes in pressure during valvular motion. At the beginning of systole, the mitral valve closes, causing Left Ventricle pressure to rise (red line). After the aortic valve opens and closes during Left Ventricle ejection, the pressure drops below the Left Atrium pressure (black line). The constant negative pressure suction is approximately 1~2 mmHg $(1\ mmHg\ =\ 0.000133\ MPa)$. This period of where the Left Ventricle pressure is negatively influenced by the lowered pressure in comparison to the Left Atrium pressure is how the mitral valve opens during diastole.

Heart rate is assumed to be 60 beats per minute, so the time period of all steps combined is set to comprise one full second. In Abaqus, the step sequences are set in the following order: initialization, diastolic, and systolic phases. The initial increment size is set to 0.025 seconds, the minimum increment size is set to 1e-30, and the max increment size is set to 0.05 seconds. The upper limit of increments is capped at 1000 increments. ABAQUS solver defaults to direct linear equation systems and Newton-based integration. The alternatives are not chosen due to their excessive and computationally-intensive run times. ABAQUS default general solution controls were adjusted to accommodate the large number of iteration attempts required for the geometric complexity of the model. The variable I_A is increased from the system default of 5 iteration attempts to 30.

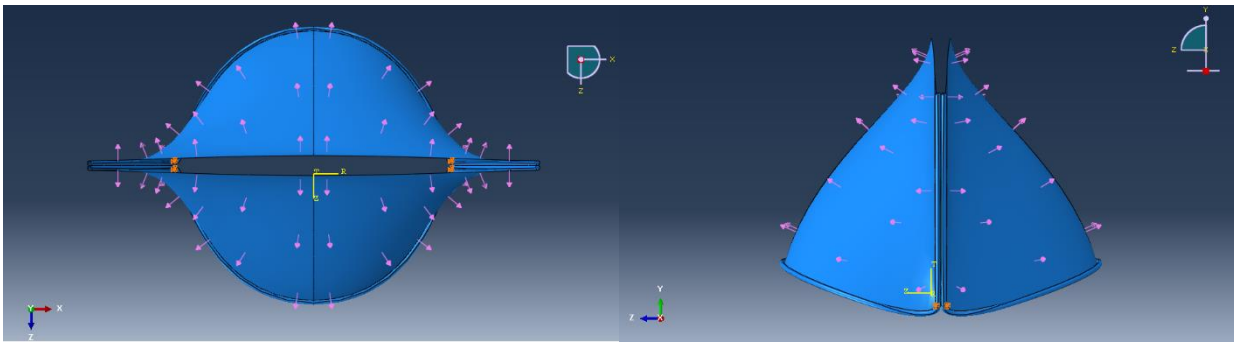

Figure 11: Pressure fields & Boundary Conditions (Diastole)

In the above step (during diastole) loads are applied to the entire surface of the leaflet and are uniform across the full surface of each bileaflet half. Pressure is a negative suction across the top surface, while the four boundary conditions, two per midsection edge, have two degrees of freedom (DOF) allowing rotation in the x and z-axis but constraining the nodes in place. Note that the heart chambers in this case are viewed upside-down, where blood flow is directed upward towards the positive y-axis.

Efforts to facilitate convergence of the solution

Enforcing Model Assembly Constraints and Contact Constraints

The model surface assembly must be programmed to have interactions between all the individual parts to simulate contact, tangential behavior, friction, shear stresses, and more. ABAQUS models contact problems by designating relevant interaction pairs as master and slave surfaces or self-contact, as detailed in [30]. General contact interactions are a tool used to model self-contact for surfaces that include multiple bodies. The contact of the surfaces is set to account for thickness. Each set of the contact pairs along the edges are defined as node regions and specified as tie interactions with restricted DOF. Contact analysis for leaflet closure is done through penalty-based friction formulations with an assumed friction coefficient of 0.3 with accordance to results from Dr. Wei Sun [19]. For the results to have significance in context of the surrounding components, boundary conditions are specified to establish a frame of reference regarding the applied pressures to the model.

Enforcing Boundary Conditions

The anterior and posterior leaflet edges of the bioprosthetic design feature upper portions near the A1, A3 and P1, P3 regions that are intended to anchor its geometry to the endocardium. Therefore, in the FE model, these areas of the leaflet will be considered fixed boundary conditions and anchor points for the frame's saddle geometry. According to [5], in the native mitral valve, the boundary conditions cannot be strictly defined to be immovable; though the name suggests otherwise, the annulus is variable, more membrane-like, and not completely circular like most bioprosthetic designs. There is no simple reference point for spatial homogeneity of the leaflet, due to the valve's dynamic nature and constant changes in position, as discussed by [2]. However, for the purposes of this FE model, it is assumed they are static and unable to slide in plane directions. Two boundary conditions are specified per leaflet half. Two are placed at the A1/A3 midsection, and likewise, the other two are placed in a symmetrical fashion near the P1/P3 region. In total, there are four static boundary conditions. Boundary condition points on the leaflet edges are fixed in all three plane directions with freedom to rotate to allow bending in the x and z-axis. The location of the central boundary conditions provides the two external frames on the sides of the leaflets a rotation constrained to the z-axis $(-\infty < z < +\infty)$. Similarly, each of the bileaflet halves are allowed rotation in the x-axis $(-\infty < x < +\infty)$.

Table 4: Final Values for Abaqus Input Data (Leaflet)

Description		*Value*	*Units*
Leaflet Material*	Poisson's Ratio	0.49	Dimensionless
	Bulk Modulus K_0	4000	MPa
	Shear Modulus	3.45	MPa
	Density	1.045e-9	kg/mm^3
	Material Constant C01	33.2	MPa
	Material Constant C10	0.101	MPa
	Incompressibility Parameter D	7e-4	1/MPa
	Fiber Stiffness K_1	10.8	MPa
	Nonlinear Fiber Stiffness K_2	48.5	MPa
	# of Local Directions	2	
	Dispersion of fibers κ	0.089	
	Thickness t	0.4	mm
	Friction coefficient	0.3	
	Transverse shear stiffness	0.01	MPa

*Sources: Values adapted from Wei Sun [19], Pham [26], and Pouch [33]

Table 5: Other Abaqus Input Data

Description		*Value*	*Units*
Step Increment	Time Period (Systole)	0.25	s
	Time Period (Diastole)	0.75	s
	Minimum Increment	1e-30	s
Load	Systole	1.33e-2	MPa
	Diastole	1.33e-4	MPa
Mesh	Quad-Structured Shell (S4R) Leaflet Seed	1.0	mm
	Quad-Sweep Shell (S4R) Frame Seed	1.0	mm

RESULTS

As a final step of the FE analysis process, the entire system must be solved numerically. The final input data is implemented into Abaqus software computational packages (see Table 3 and 4). The output can be quantified in terms of graphs, tabulated as data, or observed visually through software. Several different saddle-based geometries were tested for stress distributions, each with various levels of capability for valvular opening and closing. Much of the stress and strain experienced by the leaflets is known to occur during the earliest phases of the cardiac cycle, according to [36]. Complete loading of the valve occurs within ~5 milliseconds, with a quick transition to the fully pressurized state, according to [2]. The following images show the most successful reduction of stress during leaflet closure (Figure 12).

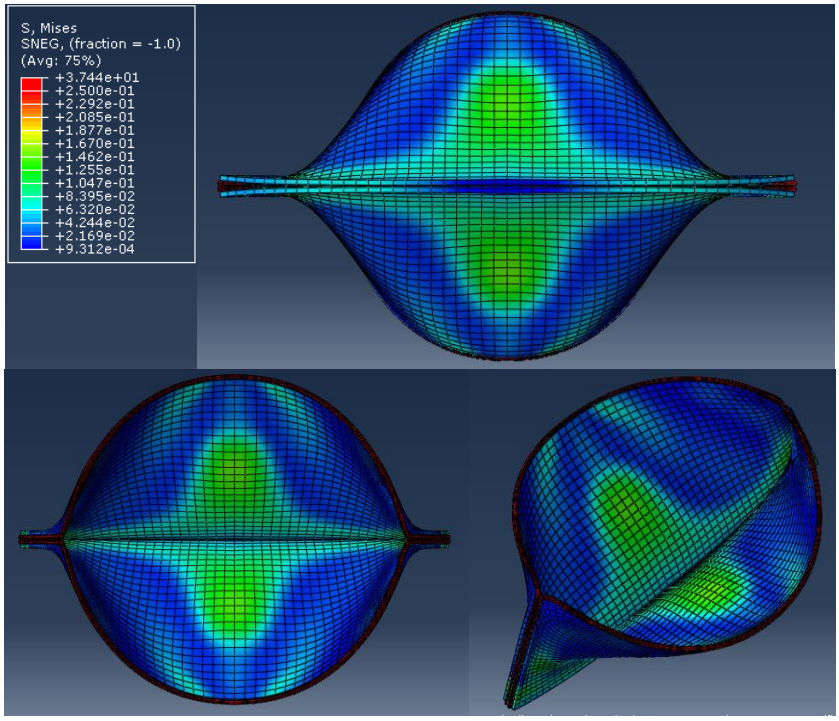

Figure 12: Model Von Mises Stress Distributions

Visualization of results with Von Mises stress mapping (MPa) after 0.05 seconds during leaflet closure in the systolic phase. The final stage of deformed bileaflet bioprosthetic viewed from top, bottom, and reverse-isometric view perspectives. Majority of stress is concentrated in the midsection belly of the leaflet, away from the leaflet tips and edges.

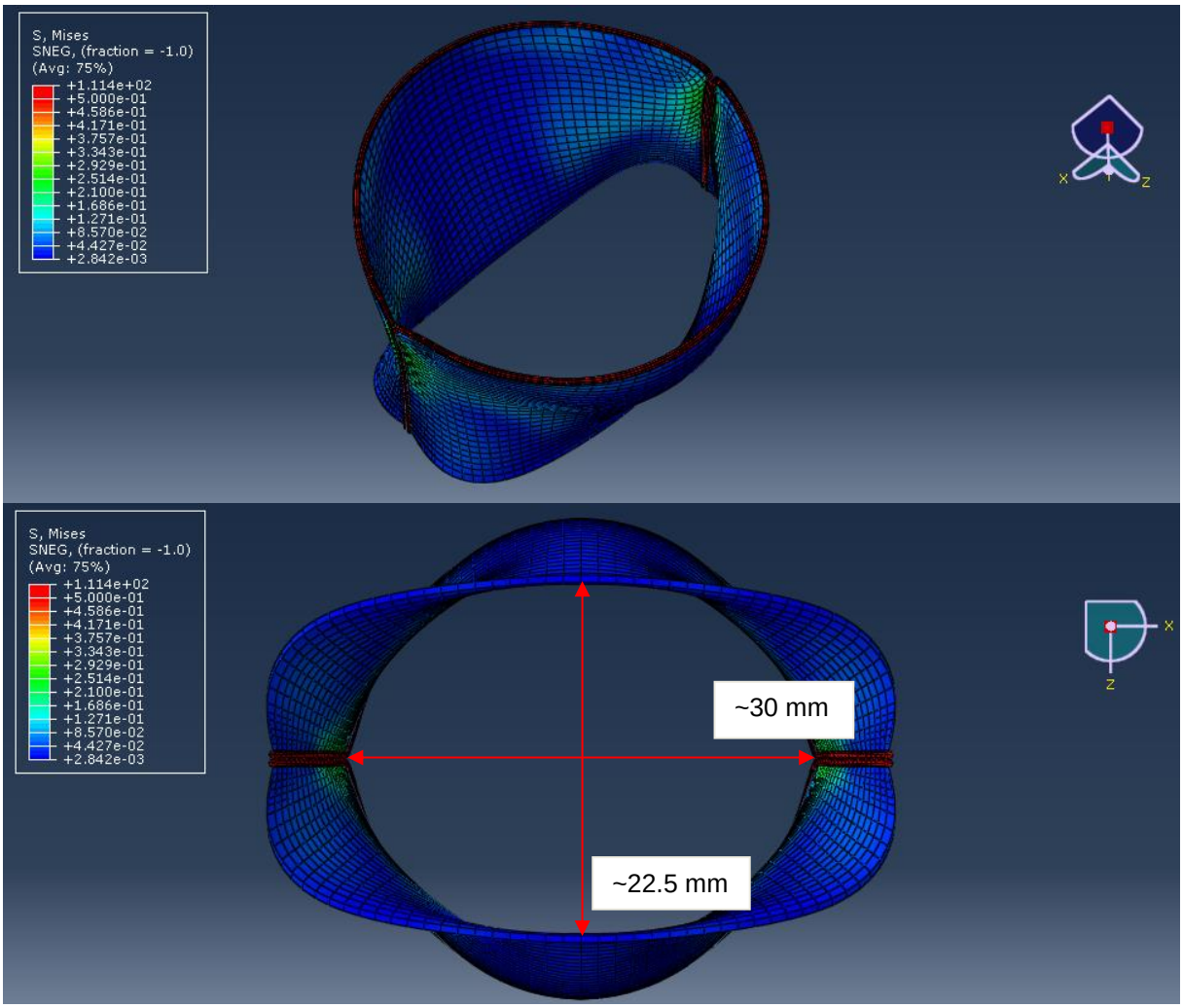

Figure 13: Maximal Opening

Von Mises stress mapping (MPa) during diastole. The saddle geometry of the valve causes the frame and leaflet halves to move in such a way that the originally flat and closed profile of the valve's narrow opening deforms into a roughly circular opening. Blood flow through the valve is maximized as a result of this elliptical opening profile. Measured using the long and short axis, the circumference of the elliptical opening is approximately 83.3 mm, and the area is approximately 530 mm^2.

Finite Element Analysis: Stress/Strain Relationships

Examining how stress and strain change over the course of the pressure simulation illuminate the anisotropic properties of the bioprosthesis design. In addition, focusing on single elements of the mesh allows for investigation into the nonplanarity of the saddle-shaped leaflet by contrasting different areas of the curvature (Figure 14). The stress and strain curves of the single elements will be plotted for the circumferential and radial directions for the first 5 milliseconds of the applied load. Stress curves in the following plots will be in units of megapascals and seconds (Strain, as a ratio of lengths, will be dimensionless). The plots were directly extracted from the Abaqus visualization module.

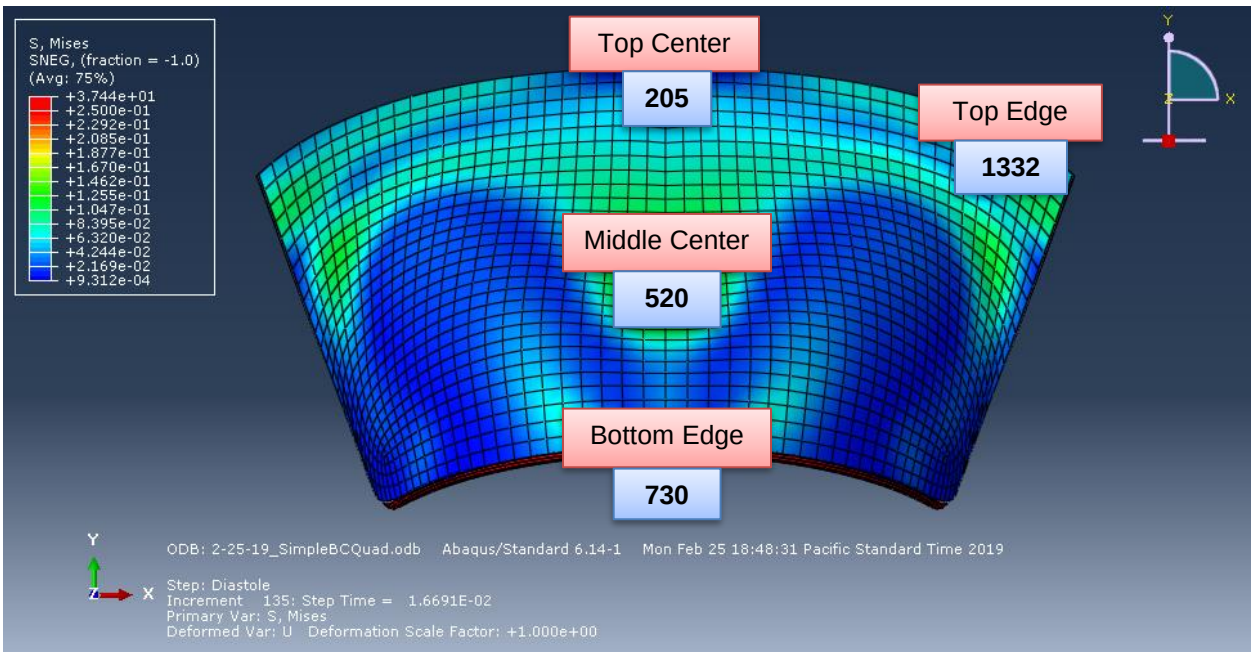

Figure 14: Mesh Locations for Single Element Study

Stress and strain curves will be generated for the element as it deforms under the simulated pressures. Each leaflet half contains 1418 elements (709 per leaflet quarter), making it a total of 2836 mesh elements for the combined model. The specified mesh elements used in the study are listed from top to bottom: #205, 1332, 520, 730. The following pages go into detail for each of the highlighted elements. Stress is measured in megapascals (MPa) and time in seconds (s).

Top Center Element Stress/Strain Curves

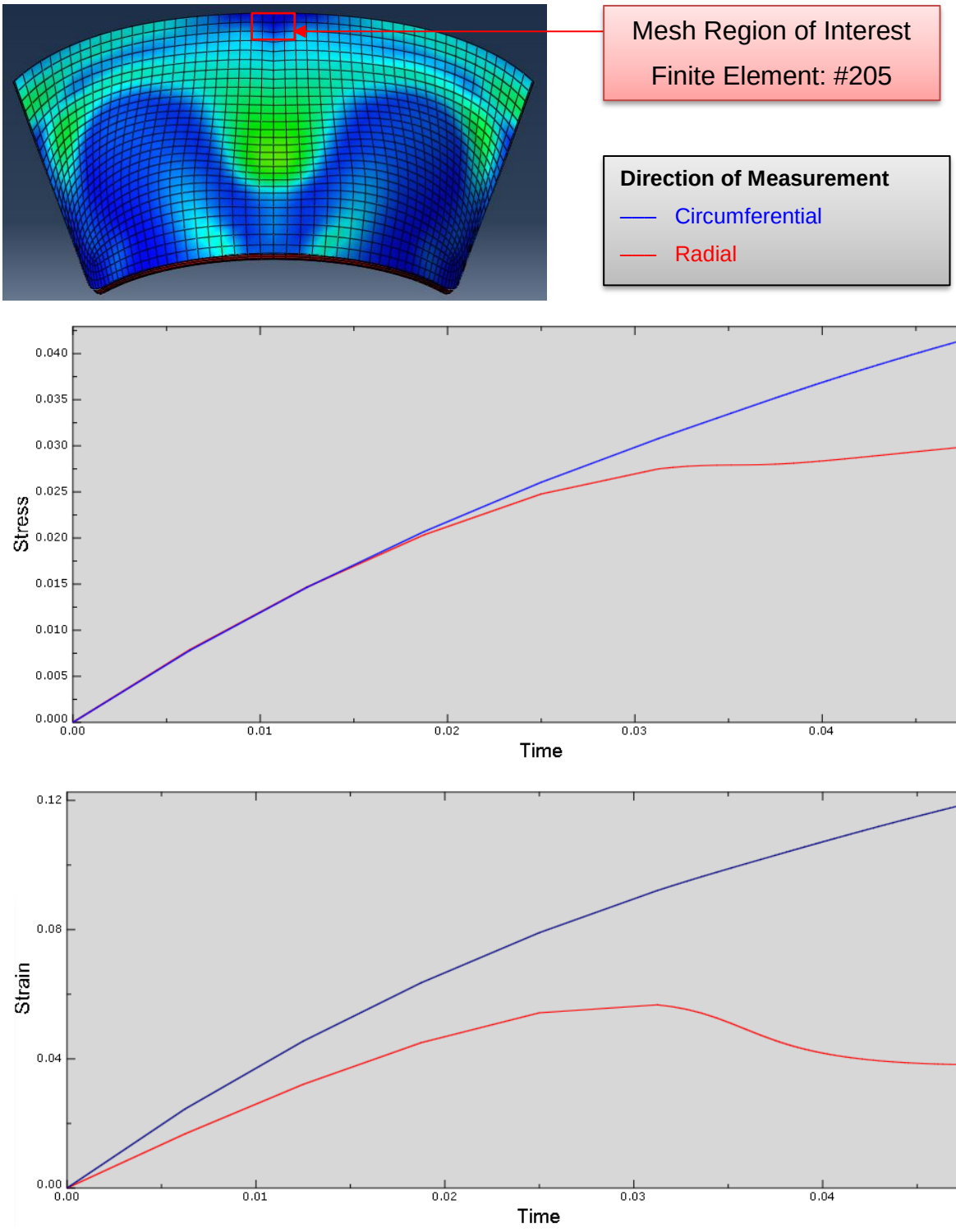

Figure 15: Top Center Element Stress/Strain Curves

Middle Center Element Stress/Strain Curves

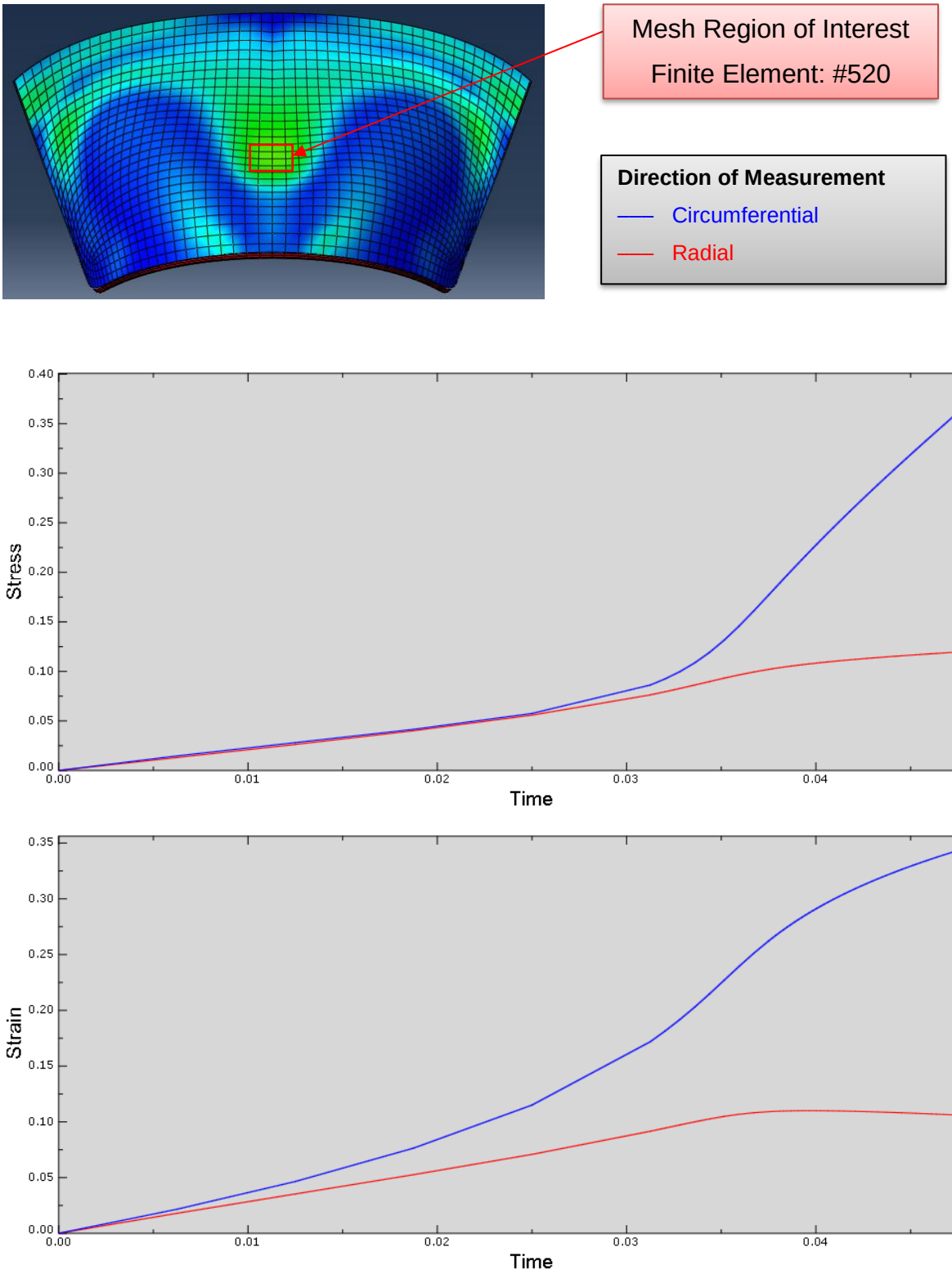

Figure 16: Middle Center Element Stress/Strain Curves

Bottom Edge Element Stress/Strain Curves

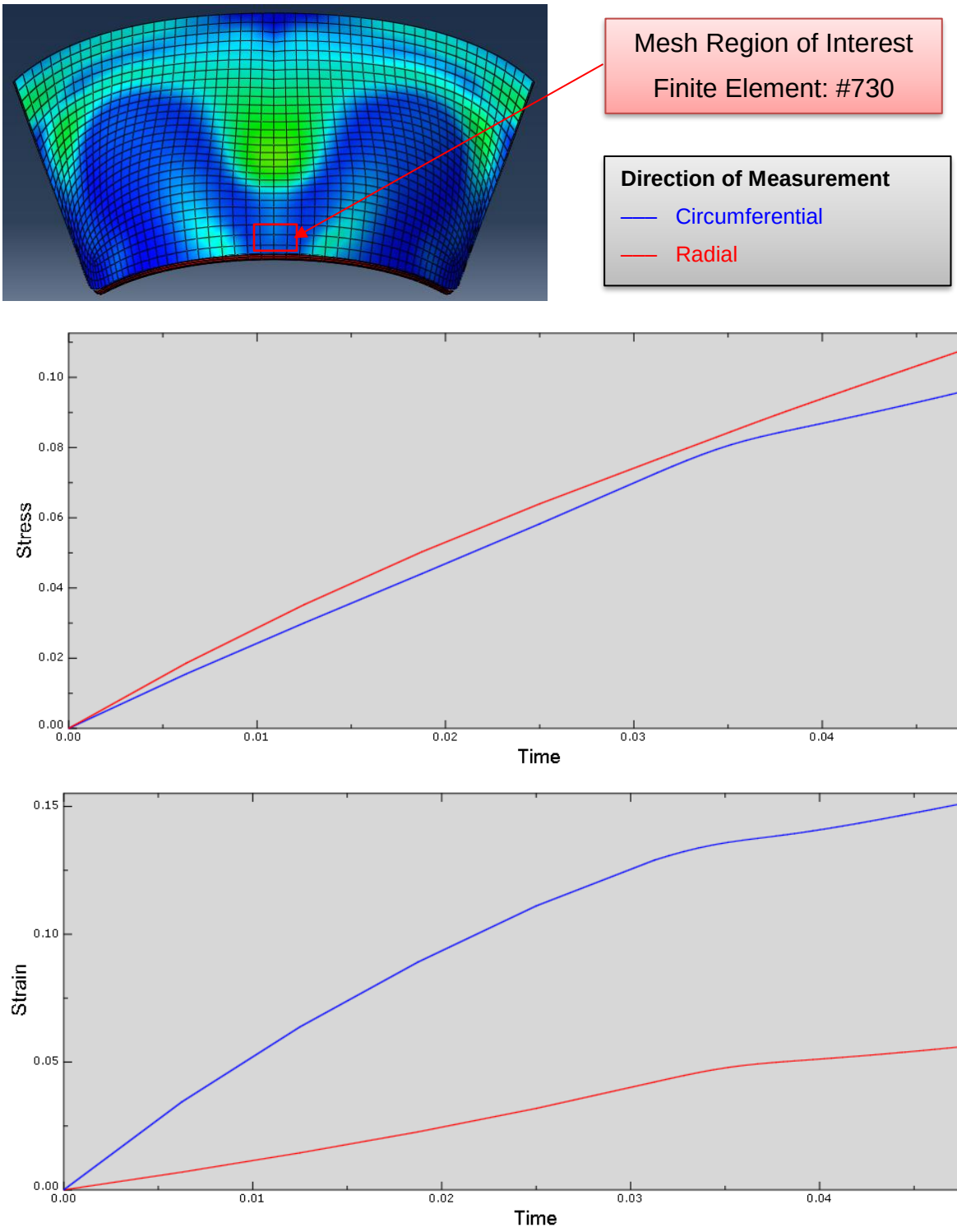

Figure 17: Bottom Edge Element Stress/Strain Curves

Top Edge Element Stress/Strain Curves

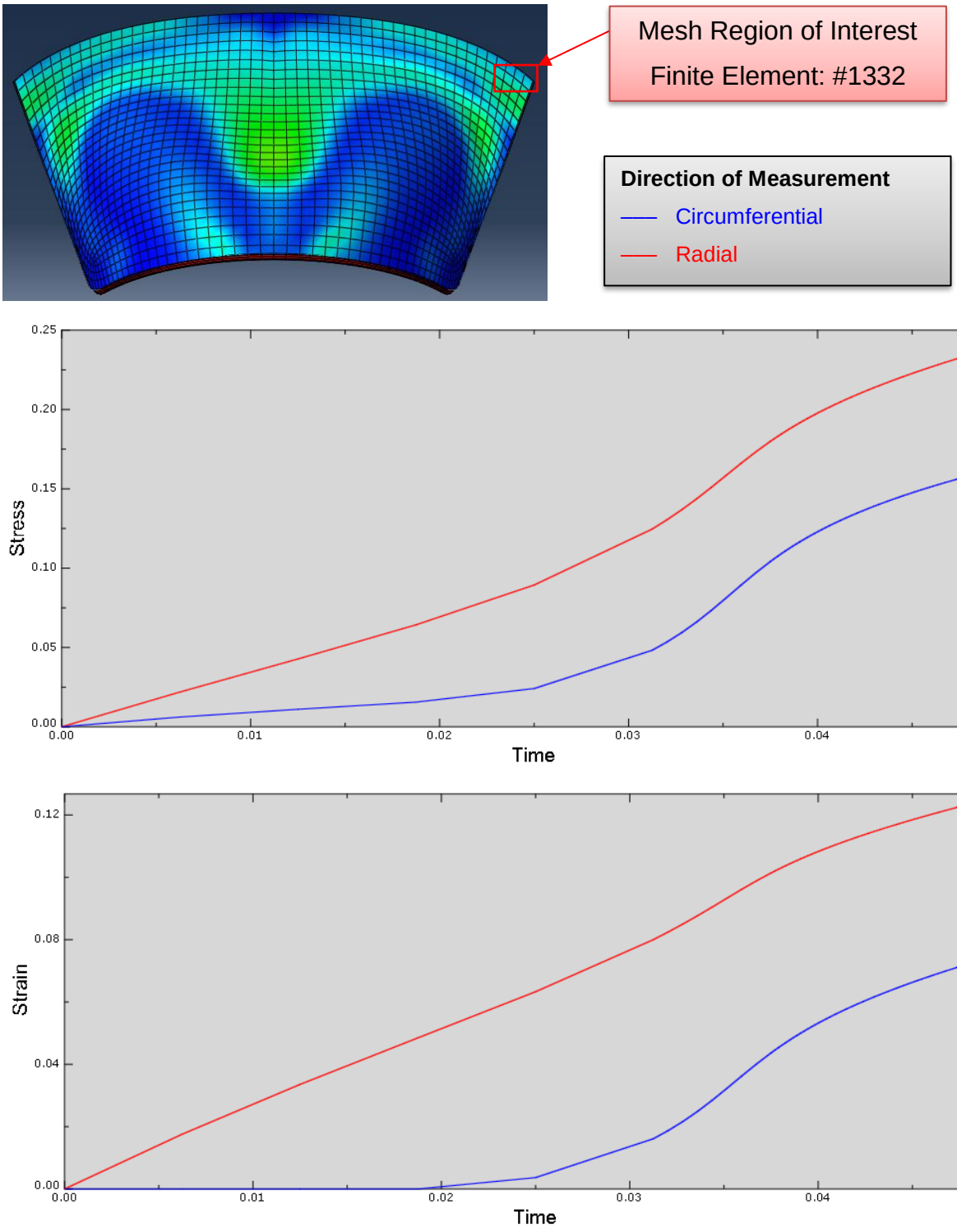

Figure 18: Top Edge Element Stress/Strain Curves

DISCUSSION

Prosthetic replacements of heart valves have saved millions of lives over the course of the last half-century. Unfortunately, like many current medical device substitutions, mitral replacements cannot entirely perform up to the standard of what the original valve can do. As long as valve bioprosthesis continue to be used extensively in replacement surgeries, it is essential that the biomechanics behind bioprosthetic mitral designs are understood thoroughly. For that purpose, the study of native biomechanical properties of the mitral valve—such as its bileaflet nature, the saddle-shaped annulus, and aligned collagen fiber orientation—using FE models under pressure simulations may provide knowledge that will improve future bioprosthetic designs.

Effects of the preferred fiber direction on stress/strain measurements

Data obtained from the results of the pressure simulations reveals a significant variation in stress/strain measurements over time in the circumferential and radial directions. Two major local directions were specified for fiber orientation in the leaflet tissue: circumferential and radial. The constitutive model used in this study set the biomechanical properties of the anterior leaflet to have an elastic modulus of 6.2 MPa in the circumferential direction and 2.1 MPa in the radial direction, meaning the circumferential stiffness is higher than the radial stiffness. Additionally, the degree of dispersion of fibers $(0 \leq \kappa \leq 1/3)$ was set to 0.089, making the leaflet fibers highly oriented along the preferred fiber directions (see Table 3).

Quantitative stress/strain plots were obtained from tracking the data of single mesh elements over the course of the first 5 milliseconds. Due to the fiber-aligned

constitutive model, the biomechanics when tracking region-specific parts of the model's mesh show that there are significant differences in magnitude, gradient, and distribution over time. At the top center elements (see Figure 15), the magnitude of stress for both circumferential and radial direction is much lower than the other areas, maxing at 0.045 MPa circumferential stress after 5 milliseconds. However, the strain experienced is average, at 0.12 for circumferential and 0.04 for radial. The circumferential strain was found to be much higher than radial strain, whereas the stress stayed roughly similar over the same timeframe. Slope of the circumferential and radial stress is similar for the first 0.03 seconds, but afterwards the radial stress curve begins to level out, whereas the circumferential stress curve continues to climb.

These results were amplified at the belly of the leaflets, where the leaflet was observed visually to bear a larger amount of circumferential stress (see Figure 16). Circumferential and radial stress start out with nearly identical values and slope for the first 0.03 seconds, but after that, the slope of the circumferential curve suddenly increases and diverges from the radial curve. The plot distribution of the middle center elements is similar the top center elements but with a higher magnitude of stress and strain. The belly of the leaflets maxed out at 0.4 MPa of circumferential stress and a strain value of 0.35 in the circumferential direction; the radial stress maxed out at 0.125 MPa and at a strain value of 0.1 in the radial direction. Overall, the circumferential stress and strain over time start out similarly in scale and slope, but eventually circumferential stress and strain begin to dominate. Additionally, a higher magnitude of circumferential stresses and strains is found within the central region of the leaflets as a result of the bileaflet saddle-shape geometry.

Conversely, measuring the stresses and strains experienced at the edges of the leaflets show a different distribution than the central elements. At the bottom edge elements (see Figure 17), circumferential stress (0.1 MPa) and radial stress (0.11 MPa) are found to have similar slopes and magnitude throughout the first 5 milliseconds of the applied load. The maximum circumferential strain (0.15) is still much larger than the radial strain (0.06) within that same timeframe, however. The overall magnitude of values measured at the bottom edges are significantly lower than the values measured at the central region. Additionally, examining the elements at the top edge (see Figure 18) show that the radial stress (0.24 MPa) and strain (0.13) values are consistently higher than the circumferential stress (0.16 MPa) and strain (0.07) values. The magnitude of these values is in between the high values measured at the center and the lower values near the top center elements. The result of measuring the stress and strains of the leaflet edges indicate a higher degree of circumferential stiffness at regions closer to the top edges of the leaflet. This is largely in contrast with the measurements taken at the center (belly) of the leaflets, in which circumferential stress and strains are higher, leading to a higher degree of radial stiffness.

Differences between saddle-shaped bileaflet geometries

Different model designs were constructed and tested across the scope of this project. The aim was to find a particular saddle-shaped geometry that reduces stress conditions at the leaflet edges when placed under the same loading conditions. This in turn would potentially help determine the reasons behind the locations of high stress concentrations that occur at the leaflet edges during the diastolic and systolic phases.

Early models featured much thinner geometry than the one presented in this paper, with sharper inward curvature along the belly of the leaflets before rising to meet at the valve coaptation zone. The angle of the initial guiding curvature of the leaflet when viewed from the side was set to 45° (measured from the positive y-axis) instead of 20°, resulting in a shorter, flatter valve along the annulus edge. The concavity of the leaflet shape was an attempt to mimic the design philosophy of the aortic valve cusps, which bend outwards from a concave shape to allow the valve to open. However, it was discovered that the bileaflet nature of the design caused this flatter geometry to have a restricted capability of opening. In addition, stress concentrations were found to heavily affect the outer tips of the leaflet near the nitinol frame supports. This resulted from the valve struggling to open but not having enough leaflet material along the central region to allow such an opening; the geometry was too thin, and the narrow corners of the opening experienced too much strain while attempting to deform into a circular shape.

This problem was solved by allow the side curvature to slightly bulge outwards into a convex shape near the belly of the leaflets, resulting in the geometry displayed in the paper results (see Figure 3). Not only did this geometry divert the stress from the opening tips, it also redirects a large portion of it across the outwardly curved belly of the leaflets during valve closure. After 0.05 seconds, maximum stress values from the belly reach 0.4 MPa, when compared to the maximum stress of 0.045 MPa near the opening edges (see Figure 15 and 16). The new bileaflet curvature design also assists in creating in the desired opening geometry, allowing the sides to deform inward and form an elliptical opening profile.

Deformation occurs in a circular shaped opening

The curved saddle-shape of the surrounding annulus allows the bileaflet bioprosthetic to deform in a way that results in an elliptical, but roughly circular-shaped opening, despite the initial nonplanar 3D saddle geometry. While closed, the state of the valve can be described as two bileaflet halves pressed together to from a narrow boundary across the coronal plane, which can be defined as a fully closed line profile. However, after the model deforms due to pressure differences between the two cardiac chambers, that said boundary begins to open, first forming a thin ellipse that then transitions into a circular shape, as shown in Figure 13. The saddle height (3.25 mm from the bottom of the saddle geometry, see Figure 3) of the saddle curvature of the annulus perimeter provides the valve its ability to deform in that way, and it can be observed by the shape of the opened valve during the diastolic phase. The inclusion of the unique saddle geometry allows for this smooth transition from its closed state. Lastly, the maximal opening of the bioprosthetic mitral valve offers the maximum amount of surface area for blood flow during ejection phase. The maximum circumference of the opening was recorded to be approximately 83.3 mm, and the maximum area was found to be approximately 530 mm^2 (see Figure 13).

Coaptation zone as a result of bileaflet saddle geometry

The anterior and posterior leaflets of the bileaflet design come together at the central divide and form extended contact with each other as a result of the 3D saddle geometry (see Figure 12). The curved semicircle shape of the opening flaps of the leaflets assists in valve closure. Whereas a two-dimensional or flat annulus would result

in a more rigid and less variable boundary, the curved nature of the bioprosthesis design in 3D space helps push the thin surfaces of the dual leaflets together to tightly shut during systole to prevent leakage of blood. The height of the semicircular flap that forms the coaptation zone was set to 7 mm (see Figure 3). Designs featuring shorter flaps were tested, but during systolic valve closure, the two halves of the bileaflet valve only partially sealed at the center of the opening, resulting in two gaps forming at the sides. The described scenario would result in retrograde flow during systole when the valve must be tightly shut. The angled, arch configuration of the bileaflet opening edge is assisted by the saddle-shape of the annulus as it moves in 3D space, pushing the two halves of the leaflet together to form a fully closed, leak-free valve.

The inclusion of the nitinol frame support

The annulus frame, due to being made of the shape memory alloy Nitinol, has properties that allow it to be dependably bent and deformed along with the complex saddle-shape of the bioprosthetic. Stent material for transcatheter delivery has very demanding requirements. While other stent supports have deformable properties, like polymer-based stents or other metallic materials, nitinol offers unique advantages that trump the other options in durability, flexibility, and biocompatibility. Even though the clinical data backing them is significant, biodegradable polymer stents currently face many challenges, including low structural integrity, biocompatibility issues, and poor delivery, according to [37]. Other metallic stent materials do not offer the unique phase transformation that nitinol undergoes during changes in temperature, and the suitability of internal body temperatures lends itself greatly towards this advantage. Nitinol exhibits

properties of superelasticity and shape-memory, allowing it to be ductile in martensitic form—but when heated, nitinol will recover the pre-deformed shape in its austenite form, as detailed in [38]. Due to the normal internal body temperature of 310 K, nitinol can utilize its thermomechanical properties to be delivered in a flexible, martensitic form (291 to 271 K), but when deployed in the body, it will recover its original shape by undergoing phase transformation to its austenite form (295 to 315 K), as detailed in Table 1. This is a key advantage of nitinol as a strong and flexible metallic alloy; it can be delivered via transcatheter while retaining its shape and durable properties.

Failure Modes

The possible errors experienced in performing data analysis are mostly attributed to geometry complexities and inability to reach convergence due to limitations placed on the tethered nature of the imposed boundary conditions. It is necessary for the model to be fixed in some form, but in doing so, artificial stress concentrations near said fixtures become inevitable. Additionally, simplifications and approximations are made to speed up the process of analysis to obtain practical solutions close to reality, but it is at the cost of accuracy. As a result, forced analysis termination of Abaqus program after simulated pressure is applied is a common failure mode due to excessive distortion of the model mesh because of said boundary conditions, and insufficient software memory to solve such complex conditions arose. Oversimplified or unrealistic material properties are another source of early analysis failure. Assumptions can be made that introducing non-homogenous, anisotropic material properties can make ideal physical simulations,

but it can fail in complex, nonlinear biomedical problems. Continued analysis of the value approximations inputted into the anisotropic tensors is required.

CONCLUSION

In this study, finite element studies were performed on a simulated bileaflet mitral bioprosthetic valve undergoing standard pressure differences of 100 mmHg during systole and a negative pressure of ~1 mmHg on the leaflet surface during diastole. As the pressure ramps over the course of 5 milliseconds, stress and strain distributions were calculated in the circumferential and radial directions, revealing an overall greater circumferential stiffness along the opening and annulus edges of the leaflet. Along the top edges, radial stress dominates; however, areas closer to the central belly of the leaflet surface shift towards greater circumferential stress. As a result of the bileaflet model's saddle-shape curvature, a greater amount of circumferential strain was experienced near central areas of bending in the model, while the top edges experienced more radial strain. Thus, overall, the leaflet edges are stiffer along the circumferential direction, while the midsections of the leaflet are stiffer in the radial direction.

The saddle-shape uniquely spreads the circumferential stress away from the edges

Unlike a flat, nonplanar model, the stress distribution patterns from a bileaflet, saddle-shaped design are shown to behave more efficiently. Due to the unique 3D geometry of the bileaflet design, the resulting circumferential stress distributions are diverted from the edges and focused towards the central region of the leaflets. The

resulting saddle-shaped bileaflet design addresses how the edges of the native leaflet geometry are known to experience a greater amount of stress. Whereas a nonplanar model would experience focused regions of stress solely at the extreme edges of the surface, the saddle-shape redirects a significant fraction of the circumferential stress to the belly of the leaflets as a result of the changes in curvature along the A2/P2 midsection of the leaflet, increasing the circumferential stiffness of the edges, and minimizing leaflet closure stress.

The fiber-aligned material model reveals higher circumferential stress/strain measurements at the bileaflet center

The data points towards a higher degree of stress experienced by the bileaflet design in the circumferential direction closer to the belly (center) of the leaflet. The peak circumferential stress values near the belly region after 5 milliseconds (0.4 MPa), as opposed to the radial stress (0.125 MPa), as shown in Figure 16, show how the circumferential stress curve greatly diverges after 3 milliseconds of the applied load. In elements closer to the bottom edges, the circumferential (0.1 MPa) and radial (0.11 MPa) stresses are roughly equivalent, but the circumferential strain remains higher than the radial strain. Circumferential strain is much higher towards the center of the leaflet, likely due to the higher degree of nonplanarity of the saddle-shaped geometry. The boundary edges of the leaflet remain higher in circumferential strain the closer you measure towards the edges of the saddle geometry. Meanwhile, in the very top edges of the leaflet near the nitinol frame side supports, radial stresses and strains begin to dominate over the circumferential stresses and strains. The conclusion of this study

establishes that the saddle-shaped design experiences a higher degree of circumferential stress towards the belly of the leaflets as a result of the fiber-aligned constitutive model. Knowledge of the directionally-dependent biomechanics behind how this design bears pressure loads may lead to future work in the creation of bileaflet bioprosthetics.

FUTURE WORK

Future work may require a higher degree of investigation into the correlation between the directionally-dependent tissue fibers and its stress distributions. Continued in-depth FE analysis on the effects of bending and contortions of the bileaflet bioprosthetic during recurrent opening/closing phases in Abaqus will be the next stage for this project. Implementing newer test data from modern studies on anisotropic material properties, while maintaining awareness of excessive distortions that could lead to tearing, will provide more insight into how the saddle-shaped annulus influences the leaflet deformation properties. Continued investigation beyond comparing circumferential and radial fiber alignment and more research into the correlation of anisotropy and regional heterogeneity along the leaflet surface would prove to be another new case of study. For the valve leaflets and nitinol frame, trying a variety of Nitinol alloy material types, non-uniformity in leaflet thickness, different pressure loads, and flexible boundary conditions should provide interesting data to investigate. The amount of powerful forces that the mitral valve leaflet is subject to is a primary reason for the importance of this data.

Studies on fiber realignment during the constantly varying physiological loads on native tissue may yield a greater understanding of how to increase the efficacy of fiber alignment in bioprosthetic engineering design. The importance of fiber direction and saddle geometry when it comes to the production of bileaflet mitral valve replacements cannot be overlooked, as it has the potential to increase the longevity of future bioprosthetics. Greater knowledge of the biomechanical properties of bileaflet bioprosthetic valves brings forth greater potential for designing safer and more durable valve replacements.

LIST OF REFERENCES

[1] K. J. Grande-Allen and J. Liao, "The Heterogeneous Biomechanics and Mechanobiology of the Mitral Valve: Implications for Tissue Engineering," *Current cardiology reports,* vol. 13, no. 2, pp. 113-120, 2011.

[2] M. S. Sacks, W. D. Merryman and D. E. Schmidt, "On the biomechanics of heart valve function," *Journal of Biomechanics,* vol. 42, no. 12, pp. 1804-1824, 2009.

[3] A. Kheradvar and A. Falahatpisheh, "The Effects of Dynamic Saddle Annulus and Leaflet Length on Transmitral Flow Patterns and Leaflet Stress on a Bileaflet Bioprosthetic Mitral Valve," *The Journal of Heart Disease,* vol. 21, pp. 225-233, 2012.

[4] B. Ramlawi and J. S. Gammie, "Mitral Valve Surgery: Current Minimally Invasive and Transcatheter Options," *Methodist Debakey Cardiovascular Journal,* vol. 12, no. 1, pp. 20-26, 2016.

[5] S. Y. Ho, "Anatomy of the mitral valve," *Heart Journal,* vol. 88, no. (Suppl 4), pp. iv5-iv10, 2002.

[6] M. Padala et al., "Saddle shape of the mitral annulus reduces systolic strains on the P2 segment of the posterior mitral leaflet," *The Annals of Thoracic Surgery,* vol. 88, no. 5, pp. 1499-1504, 2009.

[7] M. Vergnat et al., "The effect of surgical and transcatheter aortic valve replacement on mitral annular anatomy.," *The Annals of Thoracic Surgery,* vol. 95, no. 2, pp. 614-619, 2013.

[8] A. Carpentier, D. H. Adams and F. Filsoufi, Carpentier's Reconstructive Valve Surgery, Saunders, 2010.

[9] V. Prot, R. Haaverstad and B. Skallerud, "Finite element analysis of the mitral apparatus: annulus shape effect and chordal force distribution," *Biomechanics and Modeling in Mechanobiology,* vol. 8, no. 1, pp. 43-55, 2009.

[10] S. H. Alavi, A. Sinha, E. Steward, J. C. Milliken and A. Kheradvar, "Load Dependent Extracellular Matrix Organization in Atrioventricular Heart Valves;

Differences and Similiarites," *Americal Journal of Physiology - Heart and Circulatory Physiology,* vol. 309, pp. 276-284, 2015.

[11] S. H. Alavi, V. Ruiz, T. Krasieva, E. L. Botvinick and A. Kheradvar, "Characterizing the Collagen Fiber Orientation in Pericardial Leaflets Under Mechanical Loading Conditions," *Annals of Biomedical Engineering,* vol. 41, no. 3, pp. 547-561, 2013.

[12] K. May-Newman, C. Lam and F. C. Yin, "A hyperelastic constitutive law for aortic valve tissue," *Journal of Biomechanical Engineering,* vol. 131, no. 8, p. 081009, 2009.

[13] K. L. Billiar and M. S. Sacks, "Biaxial Mechanical Properties of the Natural and Glutaraldehyde Treated Aortic Valve Cusp—Part I: Experimental Results," *Journal of Biomechanical Engineering,* vol. 122, pp. 23-30, 2000.

[14] K. May-Newman and F. C. P. Yin, "A Constitutive Law for Mitral Valve Tissue," *Journal of Biomedical Engineering,* vol. 120, no. 1, pp. 38-47, 1998.

[15] E. J. Weinberg and M. R. Kaazempur-Mofrad, "On the Constitutive Models for Heart Valve Leaflet Mechanics," *Cardiovascular Engineering,* vol. 5, no. 1, pp. 37-43, 2005.

[16] E. J. Weinberg and M. R. Kaazempur-Mofrad, "A large-strain finite element formulation for biological tissues with application to mitral valve leaflet tissue mechanics," *Journal of Biomechanics,* vol. 39, pp. 1557-1561, 2006.

[17] M. S. Sacks, "Incorporation of Experimentally-Derived Fiber Orientation into a Structural Constitutive Model for Planar Collagenous Tissues," *Journal of Biomechanical Engineering,* vol. 125, no. 2, pp. 280-287, 2003.

[18] J. A. Stella and M. S. Sacks, "On the biaxial mechanical properties of the layers of the aortic valve leaflet," *Journal of Biomechanical Engineering,* vol. 129, pp. 757-766, 2007.

[19] W. Sun, A. Abad and M. S. Sacks, "Simulated Bioprosthetic Heart Valve Deformation under Quasi-Static Loading," *Journal of Biomedical Engineering,* vol. 127, pp. 905-914, 2005.

[20] E. J. Weinberg and M. R. Kaazempur-Mofrad, "A finite shell element for heart mitral valve leaflet mechanics, with large deformations and 3d constitutive material model," *Journal of Biomechanics,* vol. 40, pp. 705-711, 2007.

[21] G. Krishnamurthy et al., "Stress-Strain Behavior of Mitral Valve Leaflets in the Beating Ovine Heart," *Journal of Biomechanics,* vol. 42, no. 12, pp. 1909-1916, 2009.

[22] "How Does Nitinol Work? All about Nitinol Shape Memory and Superelasticity," Johnson Matthey Medical Components, [Online]. Available: http://jmmedical.com/resources/122/How-Does-Nitinol-Work%3F-All-About-Nitinol-Shape-Memory-and-Superelasticity.html. [Accessed 2017].

[23] D. C. Lagoudas, Z. Bo, M. A. Qidwai and P. B. Entchev, "SMA_UM: User Material Subroutine for Thermomechanical Constitutive Model of Shape Memory Alloys," 2003.

[24] M. A. Qidwai and D. C. Lagoudas, "Numerical implementation of a shape memory alloy thermomechanical constitutive model using return mapping algorithms," *International Journal for Numerical Methods in Engineering,* vol. 47, no. 6, pp. 1123-1168, 2000.

[25] G. A. Holzapfel, T. C. Gasser and R. W. Ogden, "A New Constitutive Framework for Arterial Wall Mechanics and a Comparative Study of Material Models," *Journal of Elasticity,* vol. 61, pp. 1-48, 2000.

[26] T. Pham et al., "Finite Element Analysis of Patient-Specific Mitral Valve with Mitral Regurgitation," *Cardiovascular Engineering and Technology,* vol. 8, no. 1, pp. 3-16, 2017.

[27] W. Sun and M. S. Sacks, "Finite element implementation of a generalized Fung-elastic constitutive model for planar soft tissues," *Biomechanics and Modeling in Mechanobiology,* vol. 4, no. 2-3, pp. 190-199, 2005.

[28] G. A. Ateshian and K. D. Costa, "A Frame-Invariant Formulation of Fung Elasticity," *Journal of Biomechanics,* vol. 42, no. 6, pp. 781-785, 2009.

[29] F. Irgens, Continuum Mechanics, Springer, 2008.

[30] Dassault Systemes, "ABAQUS 6.13 Documentation," [Online]. Available: http://dsk.ippt.pan.pl/docs/abaqus/v6.13/index.html. [Accessed 2019].

[31] R. W. Ogden and G. A. Holzapfel, Mechanics of biological tissue, Springer, 2006.

[32] P. Boonvisut and M. C. Cavusoglu, "Estimation of Soft Tissue Mechanical Parameters from Robotic Manipulation Data," *IEEE ASME Trans Mechatron.,* vol. 18, no. 5, pp. 1602-1611, 2013.

[33] A. M. Pouch et al., "Semi-automated mitral valve morphometry and computational stress analysis using 3D ultrasound," *Journal of Biomechanics,* vol. 45, no. 5, pp. 903-907, 2012.

[34] H. Masugata et al., "Comparison of left ventricular diastolic filling with myocyte bulk modulus using Doppler echocardiography and acoustic microscopy in pressure-overload left ventricular hypertrophy and cardiac amyloidosis," *Clinical Cardiology,* vol. 23, no. 2, pp. 115-122, 2000.

[35] R. E. Klabunde, "Cardiovascular Physiology Concepts: Cardiac Cycle," [Online]. Available: https://www.cvphysiology.com/Heart%20Disease/HD002. [Accessed 2018].

[36] A. Hasan et al., "Biomechanical properties of native and tissue engineered heart valve constructs," *Journal of Biomechanics,* vol. 47, no. 9, pp. 1949-1963, 2014.

[37] C. Wiltz, "Polymer vs. Metal: The Battle of Bioresorbable Stents," Medical Device and Diagnostic Industry, [Online]. Available: https://www.mddionline.com/polymer-vs-metal-battle-bioresorbable-stents. [Accessed 2019].

[38] "Nitinol: The Flexible Friend," Verdict Medical Devices, 15 July 2010. [Online]. Available: https://www.medicaldevice-network.com/features/feature90266/. [Accessed 2019].

[39] A. Rafsanjani, "Writing User Subroutines with Abaqus," [Online]. Available: http://imechanica.org/node/7576. [Accessed 2018].

APPENDIX

Appendix A: UMAT Subroutine implementation in Abaqus

Tabular data used in this study were adapted from Lagoudas' Shape-Memory Alloy Manual [23] and Qidwai [24].

Table 6: SMA Material Input Parameters

User Material Parameter	Description	Value
IPHASE	phase of material (austenite=1, martensite=2)	1.0
MODEL	The constitutive model (Lagoudas=2)	2.0
TOL	Convergence criterion tolerance (termination if martensitic volume fraction increment is less than TOL)	1.0E-8
xi0	Initial value of martensitic volume fraction	0.0
NELMTP	Number of integration points	16.0
EA	Young's modulus, austenite (Pa)	70.0E3
EM	Young's modulus, martensite (Pa)	30.0E3
nu	Poisson's ratio	0.33
alphaA	Thermal expansion coefficient of austenite, (K^{-1})	22.0E-6
alphaM	Thermal expansion coefficient of austenite, (K^{-1})	10.0E-6
Mos	Martensitic start temperature (K)	291.0
Mof	Martensitic finish temperature (K)	271.0
Aos	Austenitic start temperature (K)	295.0
Aof	Austenitic finish temperature (K)	315.0
H	Maximum transformation strain	0.05
rDs0A	Austenitic stress influence coefficient (Pa K^{-1})	-0.35E6
rDs0M	Martensitic stress influence coefficient (Pa K^{-1})	-0.35E6

*Adapted from Lagoudas' Shape Memory Alloy User Manual [23] and Qidwai [24].

Table 7: UMAT Input/Output Parameters

Relevant Input Parameters	Description
STRAN (NTENS)	Components of total strain tensor
DSTRAN (NTENS)	Increment of strain tensor
TIME (1)	Step time value at start of current increment
TIME (2)	Total time at start of current increment
TEMP	Temperature at start of increment
DTEMP	Increment of temperature
NDI	Number of direct stress components at current integration point
NSHR	Number of shear stress components at current integration point
NTENS	Size of stress/strain component array (NDI + NSHR)
NSTATV	Number of solution dependent state variables
NPROPS	Number of material constants
PROPS (NPROPS)	Array of material constants

Relevant Output Parameters	Description
DDSDDE (NTENS, NTENS)	Array of tangent stiffness matrix components $\partial\sigma/\partial\varepsilon$
STRESS (NTENS)	Array of stress tensor components at start of increment, and updated components at end of increment (input/output)
STATEV (NSTATV)	Array of solution dependent state variables. Provided to subroutine at start of increment as input, updated and returned at end of increment as output.

*Adapted from Lagoudas' Shape Memory Alloy User Manual [23].

Appendix B: FEM & UMAT Mathematical Models in Abaqus

As an overview, the finite element method (FEM) is a discretization of a mathematical model into simple, finite elements. It is the preferred numerical way to solve partial differential equations for engineering problems and simulation of biomedical systems. Through computational modeling in software like Abaqus, this project simulates the pressures experienced by mitral valves to measure stress distributions along the leaflet surface. There are four main steps to the FEM:

I. Spatial discretization into finite elements
II. Assembling linear equation systems
III. Imposing boundary conditions
IV. Solving the system for unknowns

Computational packages like Abaqus are built to deal with these four steps by generating a FE mesh, assigning material properties, applying loads, fixtures and interactions, and as a final step, submitting the job to the computational program for analysis.

Mesh generation segments the model under study into discretized elements. For example, the segments can be single element blocks that all combine to create a unified mesh. In this study, one-fourth of the leaflet model is meshed with single element quadratic tetrahedrons. Key inflection points for the curved edge of the annulus are described as 3D coordinates measured from the origin [(x, y, z) = 0, 0, 0] located at the bottom-center of the model (Figure 19). Major point locations are described below: E1 (-23.5, 19, 0.5), P1 (-17, 1, 0.5), E2 (0, 3.25, 15).

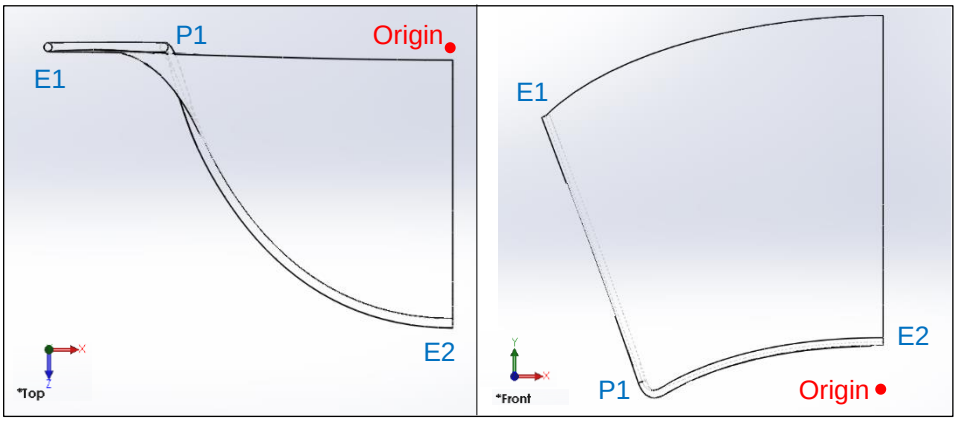

Figure 19: Placement of the main control points of the annulus

One-quarter of the bioprosthetic design. Construction was performed in Solidworks. The first image on the left is viewed from the top, while the second on the right is a view of the front. The origin at (0, 0, 0) is located at the bottom center of the full model.
Point locations: E1 (-23.5, 19, 0.5), P1 (-17, 1, 0.5), E2 (0, 3.25, 15)

Mesh density, or the element size, plays a part in running simulations in Abaqus. The finer the mesh seed, the more accurate the analysis will be, but at the expense of processing time and computing resources. When defining a mesh element type, geometric order can be specified. In this study, mesh analysis is performed using linear geometric order, where deformation follows the standard linear equation ($Ax + b$), as opposed to quadratic geometric order, where deformation along the edge follows a quadratic function ($Ax^2 + Bx + C$). In the case of large deformations, quadratic elements are more accurate. However, the simplification of the singular mesh elements will speed up processing time while remaining a decent approximation of the deformation.

Due to the switch in upward and downward curvature that is characteristic of saddle geometry, a full leaflet model proved difficult to fully create as a single continuous part. To reduce the complexity, the model was first constructed in quarters which would be mirrored to assemble the full geometry. Node constraints were implemented to tie the surfaces together at the edges to create the full model.

There are no units in Abaqus; thus, all parameter values in Abaqus must stay consistent. The following table lists the SI units used for all study analysis runs.

Table 8: English Engineering SI Units

Measurement	Units
Length	millimeters (mm)
Mass	kilograms (kg)
Time	seconds (s)
Force	newton (N)
Temperature	degree Kelvin (K)
Pressure	megapascal (MPa, or N/mm^2, or $kg*mm/s^2$)

A thermomechanical constitutive model is a mathematical description of how the material responds to various loadings with a dependence on temperature. UMAT subroutines are implemented into ABAQUS at the job submission phase of the analysis.

General Form of a UMAT subroutine header (Adapted from Lagoudas [23]):

```
      SUBROUTINE UMAT(STRESS,STATEV,DDSDDE,SSE,SPD,SCD,
     1 RPL,DDSDDT,DRPLDE,DRPLDT,STRAN,DSTRAN,TIME,DTIME,
     2 TEMP,DTEMP,PREDEF,DPRED,CMNAME,NDI,NSHR,NTENS,NSTATV,
     3 PROPS,NPROPS,COORDS,DROT,PNEWDT,CELENT,DFGRDO,
     4 DFGRD1,NOEL,NPT,LAYER,KPST,KSTEP,KINC)
C
      INCLUDE 'ABA_PARAM.INC'
C
      CHARACTER*8 CMNAME
      DIMENSION STRESS(NTENS),STATEV(NSTATV),
     1 DDSDDE(NTENS,NTENS),DDSDDT(NTENS),DRPLDE(NTENS),
     2 STRAN(NTENS),DSTRAN(NTENS),TIME(2),PREDEF(1),DPRED(1),
     3 PROPS(NPROPS),COORDS(3),DROT(3,3),DFGRD0(3,3),DFGRD1(3,3)

      *user coding to define state variables*
      END
```

Not all the above parameters are required for the relevant UMAT subroutine for the shape memory alloy, Nitinol. We can simplify it to this using the applicable ones for strain/stress analysis. As noted by [39], all UMAT subroutines, the quantities for stress, SDVs, and the material Jacobian must be defined. After the header, the code dimensions the local arrays by defining constants by parameters.

Elasticity rate equation used in template below, shown by [39]:

- Isothermal elasticity equation (with Lamé's constants):

$$\sigma_{ij} = \lambda \delta_{ij} \varepsilon_{kk} + 2\mu \varepsilon_{ij}$$

- Non-isothermal elasticity equation:

$$\sigma_{ij} = \lambda(T) \delta_{ij} \varepsilon_{kk} + 2\mu(T) \varepsilon_{ij}, \quad \text{where } \varepsilon_{ij} = \varepsilon_{ij} - \alpha T \delta_{ij}$$

UMAT Subroutine for Nitinol – Final Version

```
      SUBROUTINE UMAT(STRESS,STATEV,DDSDDE,STRAN,DSTRAN,
     1 TIME,DTIME,TEMP,DTEMP,CMNAME,NDI,NSHR,NTENS,NSTATV,
     2 PROPS,NPROPS)
C
      INCLUDE 'ABA_PARAM.INC'
C
      CHARACTER*8 CMNAME
      DIMENSION STRESS(NTENS),STATEV(NSTATV),DDSDDE(NTENS,NTENS),
     1 STRAN(NTENS),DSTRAN(NTENS),TIME(2),PROPS(NPROPS)

C LOCAL ARRAYS
C ----------------------------------------------------------------
C EELAS - ELASTIC STRAINS
C ETHERM - THERMAL STRAINS
C DTHERM - INCREMENTAL THERMAL STRAINS
C DELDSE - CHANGE IN STIFFNESS DUE TO TEMPERATURE CHANGE
```

```
C ---------------------------------------------------------------
      DIMENSION EELAS(6), ETHERM(6), DTHERM(6), DELDSE(6,6)
C
      PARAMETER(ZERO=0.D0, ONE=1.D0, TWO=2.D0, THREE=3.D0, SIX=6.D0)
C ---------------------------------------------------------------
C UMAT FOR ISOTROPIC THERMO-ELASTICITY WITH LINEARLY VARYING
C MODULI - CANNOT BE USED FOR PLANE STRESS
C ---------------------------------------------------------------
C PROPS(1) - E(T0)
C PROPS(2) - NU(T0)
C PROPS(3) - T0
C PROPS(4) - E(T1)
C PROPS(5) - NU(T1)
C PROPS(6) - T1
C PROPS(7) - ALPHA
C PROPS(8) - T_INITIAL
C ELASTIC PROPERTIES AT START OF INCREMENT
C
      FAC1=(TEMP-PROPS(3))/(PROPS(6)-PROPS(3))
      IF (FAC1 .LT. ZERO) FAC1=ZERO
      IF (FAC1 .GT. ONE) FAC1=ONE
      FAC0=ONE-FAC1
      EMOD=FAC0*PROPS(1)+FAC1*PROPS(4)
      ENU=FAC0*PROPS(2)+FAC1*PROPS(5)
      EBULK3=EMOD/(ONE-TWO*ENU)
      EG20=EMOD/(ONE+ENU)
      EG0=EG20/TWO
      ELAM0=(EBULK3-EG20)/THREE
C
C ELASTIC PROPERTIES AT END OF INCREMENT
C
      FAC1=(TEMP+DTEMP-PROPS(3))/(PROPS(6)-PROPS(3))
      IF (FAC1 .LT. ZERO) FAC1=ZERO
      IF (FAC1 .GT. ONE) FAC1=ONE
      FAC0=ONE-FAC1
      EMOD=FAC0*PROPS(1)+FAC1*PROPS(4)
      ENU=FAC0*PROPS(2)+FAC1*PROPS(5)
```

```
      EBULK3=EMOD/(ONE-TWO*ENU)
      EG2=EMOD/(ONE+ENU)
      EG=EG2/TWO
      ELAM=(EBULK3-EG2)/THREE
C
C ELASTIC STIFFNESS AT END OF INCREMENT AND STIFFNESS CHANGE
C
      DO K1=1,NDI
         DO K2=1,NDI
            DDSDDE(K2,K1)=ELAM
            DELDSE(K2,K1)=ELAM-ELAM0
         END DO
         DDSDDE(K1,K1)=EG2+ELAM
         DELDSE(K1,K1)=EG2+ELAM-EG20-ELAM0
      END DO
      DO K1=NDI+1,NTENS
         DDSDDE(K1,K1)=EG
         DELDSE(K1,K1)=EG-EG0
      END DO
C
C CALCULATE THERMAL EXPANSION
C
      DO K1=1,NDI
         ETHERM(K1)=PROPS(7)*(TEMP-PROPS(8))
         DTHERM(K1)=PROPS(7)*DTEMP
      END DO
      DO K1=NDI+1,NTENS
         ETHERM(K1)=ZERO
         DTHERM(K1)=ZERO
      END DO
C
C CALCULATE STRESS, ELASTIC STRAIN AND THERMAL STRAIN
C
      DO K1=1, NTENS
         DO K2=1, NTENS
            STRESS(K2)=STRESS(K2)+DDSDDE(K2,K1)*(DSTRAN(K1)-DTHERM(K1))
     1                                 +DELDSE(K2,K1)*( STRAN(K1)-ETHERM(K1))
```

```
        END DO
        ETHERM(K1)=ETHERM(K1)+DTHERM(K1)
        EELAS(K1)=STRAN(K1)+DSTRAN(K1)-ETHERM(K1)
    END DO
C
C STORE ELASTIC AND THERMAL STRAINS IN STATE VARIABLE ARRAY
C
    DO K1=1, NTENS
        STATEV(K1)=EELAS(K1)
        STATEV(K1+NTENS)=ETHERM(K1)
    END DO
    RETURN
END
```

Source code: Unified Constitutive Model for SMAs [23] and Writing User Subroutines with ABAQUS [39].

Abaqus Input File – What is entered into the Abaqus program

```
**ABAQUS NiTi Input file (.inp)
*HEADING
NiTi SMA

*MATERIAL, NAME = SMA
*DENSITY 6450.0
*SPECIFIC HEAT 329.0
*CONDUCTIVITY 22.0
*DEPVAR 100
*USER MATERIAL, DIMENSION(1:24)
USER MATERIAL = 1.0 2.0 1.0E-8 0.0 16.0 70.0E9 30.0E9 0.33 22.0E-6 291.0 271.0 295.0 315.0 0.05 -
0.35E6 -0.35E6 0.0 0.0 0.0 0.0 0.0 0.0 1.0

**The following material parameters are defined:
**IPHASE,MODEL,TOL,xi0,NELMTP,EA,EM,nu,
**alphaA,alphaM,Mos,Mof,Aos,Aof,H,rDs0A,
**rDs0M,epstr11,epstr22,epstr33,2epstr23,2epstr13,2epstr12,FRULE
```

Source code: Unified Constitutive Model for SMAs [23]